

Flavor-dependent long-range neutrino interactions in DUNE & T2HK: alone they constrain, together they discover

Masoom Singh, ^{a,b} Mauricio Bustamante ^c and Sanjib Kumar Agarwalla ^{a,d,e}

^a*Institute of Physics, Sachivalaya Marg, Sainik School Post, Bhubaneswar 751005, India*

^b*Department of Physics, Utkal University, Vani Vihar, Bhubaneswar 751004, India*

^c*Niels Bohr International Academy, Niels Bohr Institute, University of Copenhagen, DK-2100 Copenhagen, Denmark*

^d*Homi Bhabha National Institute, Training School Complex, Anushakti Nagar, Mumbai 400094, India*

^e*Department of Physics & Wisconsin IceCube Particle Astrophysics Center, University of Wisconsin, Madison, WI 53706, U.S.A.*

E-mail: masoom@iopb.res.in, mbustamante@nbi.ku.dk, sanjib@iopb.res.in

ABSTRACT: Discovering new neutrino interactions would represent evidence of physics beyond the Standard Model. We focus on new flavor-dependent long-range neutrino interactions mediated by ultra-light mediators, with masses below 10^{-10} eV, introduced by new lepton-number gauge symmetries $L_e - L_\mu$, $L_e - L_\tau$, and $L_\mu - L_\tau$. Because the interaction range is ultra-long, nearby and distant matter — primarily electrons and neutrons — in the Earth, Moon, Sun, Milky Way, and the local Universe, may source a large matter potential that modifies neutrino oscillation probabilities. The upcoming Deep Underground Neutrino Experiment (DUNE) and the Tokai-to-Hyper-Kamiokande (T2HK) long-baseline neutrino experiments will provide an opportunity to search for these interactions, thanks to their high event rates and well-characterized neutrino beams. We forecast their probing power. Our results reveal novel perspectives. Alone, DUNE and T2HK may strongly constrain long-range interactions, setting new limits on their coupling strength for mediators lighter than 10^{-18} eV. However, if the new interactions are subdominant, then both DUNE and T2HK, together, will be needed to discover them, since their combination lifts parameter degeneracies that weaken their individual sensitivity. DUNE and T2HK, especially when combined, provide a valuable opportunity to explore physics beyond the Standard Model.

KEYWORDS: Neutrino Mixing, New Gauge Interactions, New Light Particles, Non-Standard Neutrino Properties

ARXIV EPRINT: [2305.05184](https://arxiv.org/abs/2305.05184)

Contents

1	Introduction	1
2	Flavor-dependent long-range neutrino interactions	4
2.1	Gauged lepton-number symmetries	4
2.2	Long-range matter potential	5
2.3	Neutrino oscillation probabilities under long-range interactions	7
2.4	Existing limits	8
3	Long-range interactions in DUNE and T2HK	9
3.1	Overview of the experiments	9
3.1.1	DUNE	10
3.1.2	T2HK	11
3.2	Oscillation probabilities	11
3.3	Event rates	12
4	Projected constraints and discovery potential	14
4.1	Statistical methods	14
4.2	Projected constraints on long-range interactions	18
4.3	Discovering subdominant long-range interactions	20
5	Summary and outlook	23
A	Effects of long-range interactions on neutrino oscillation parameters	24
B	Effects of oscillation parameter uncertainties on constraints	25
C	Constraints assuming inverted mass ordering	26
D	Normalization errors in event rates	27

1 Introduction

Discovering a new fundamental interaction would be striking evidence of physics beyond the Standard Model. Yet, because new interactions are likely feeble, they are difficult to detect. And because they may manifest in a variety of ways, they are difficult to search for comprehensively. So far, there is no evidence for them, despite a long history of searches, though there are stringent limits on their strength [11–16].

Starting in the 2030s, the next-generation long-baseline neutrino experiments, Deep Underground Neutrino Experiment (DUNE) [17] and Tokai-to-Hyper-Kamiokande

(T2HK) [18, 19], presently under construction, will bring about an opportunity to search for new physics, via neutrinos, more incisively than ever before. Neutrinos have immense potential to reveal new physics [20–24]. DUNE (e.g., refs. [25–37]) and T2HK (e.g., refs. [38–45]) target this potential via rich physics programs, both within the standard neutrino paradigm and beyond it, that stem from their high expected event rates and well-characterized neutrino beams. We focus on their capability to look for new neutrino-matter interactions: because, in the Standard Model, neutrinos interact only weakly, the presence of an additional neutrino interaction may be more easily spotted, even if it is feeble.

We consider flavor-dependent neutrino-matter interactions, originally introduced in refs. [46–50], and explored and constrained in earlier literature, e.g., in refs. [1–3, 7, 8, 38, 51–65]. Two reasons motivate our choice. First, if these interactions are long-range, i.e., if they act across long distances, then large collections of nearby and distant matter may source a sizable matter potential that affects neutrino flavor oscillations appreciably. Thus, we concentrate on interactions mediated by new, ultra-light mediators, with masses below 10^{-10} eV, that subtend ultra-long interaction ranges. Second, the flavor-dependent interactions we consider are born from gauging, anomaly-free, global symmetries of the Standard Model [66–71]: $L_e - L_\mu$, $L_e - L_\tau$, and $L_\mu - L_\tau$, where L_e , L_μ , and L_τ are the electron, muon, and tau lepton numbers. This makes them arguably natural and economical extensions of the Standard Model. Gauging each one introduces a single new neutral vector boson that mediates new neutrino interactions with electrons or neutrons (interactions with other particles are suppressed, as we elaborate on later).

Previous works have explored the sensitivity of existing and future long-baseline neutrino experiments to flavor-dependent long-range interactions. However, they either fixed the interaction range, typically to be equal to the Sun-Earth distance (see, e.g., ref. [56]), or considered mediator masses only as small as about 10^{-18} eV (see, e.g., ref. [1]). We abandon both limitations and explore mediator masses down to 10^{-35} eV. Doing so opens up a largely unexplored regime of ultra-long-range interactions. As pointed out in ref. [7], a mediator this light allows for electrons and neutrons in the Earth, Moon, Sun, Milky Way, and the cosmological distribution of matter to affect neutrino oscillations. To make our forecasts realistic, we base them on detailed simulations of DUNE and T2HK, including their different detection channels, efficiency, backgrounds, and run times.

Figure 1 conveys the novel perspectives revealed by our work. It shows the first half of our main results, concerning constraints: *separately or, as in figure 1, together, DUNE and T2HK may place the strongest constraints on long-range interactions, especially for mediators lighter than 10^{-18} eV.* (Future sensitivity from flavor measurements of high-energy astrophysical neutrinos in the IceCube-Gen2 neutrino telescope might be comparable [7], but, for now, they are subject to large uncertainties in the neutrino flux, not pictured in figure 1, unlike the constraints from DUNE and T2HK.) The other half of our main results, not contained in figure 1, concerns discovery. We find that, separately, DUNE and T2HK will likely be unable to discover subdominant flavor-dependent long-range neutrino interactions, due to degeneracies between their effect on neutrino oscillations and that of the standard mixing parameters. Yet, *together, their complementary capabilities may lift degeneracies and enable the discovery of the new interactions; see figure 7.* Below, we elaborate on these perspectives.

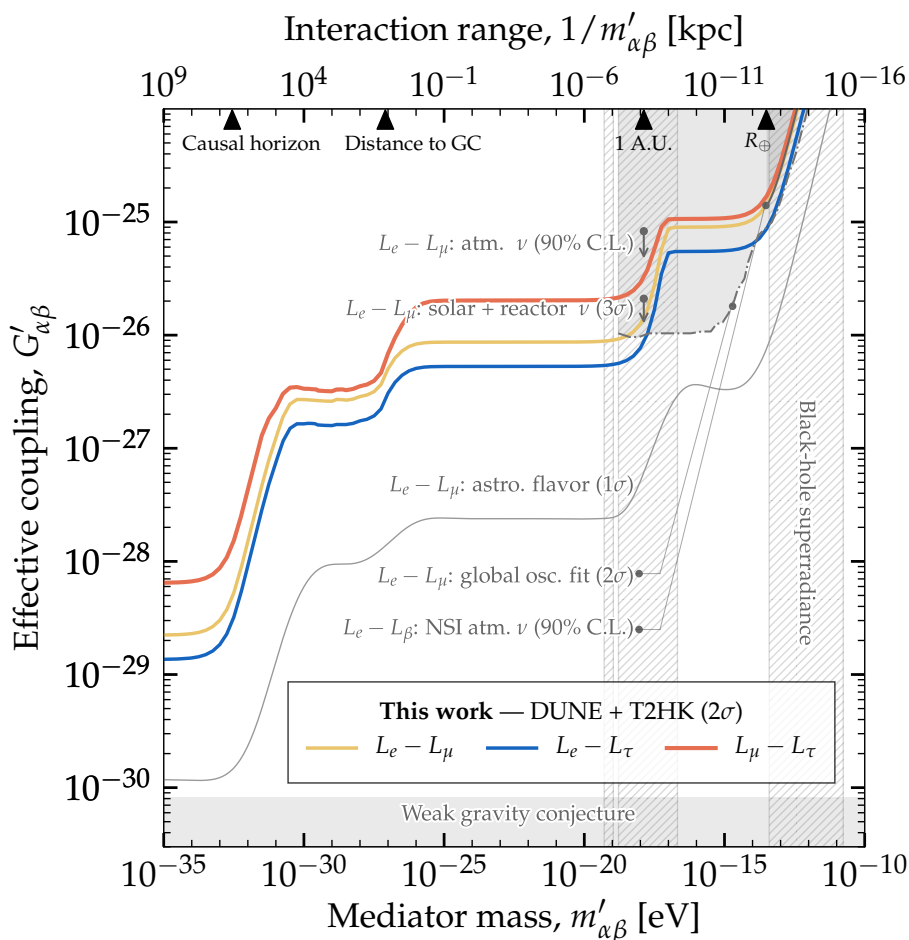


Figure 1. Projected upper limits on the effective coupling, $G'_{\alpha\beta}$ (eq. (2.7)), of the new boson, $Z'_{\alpha\beta}$, with mass $m'_{\alpha\beta}$, that mediates flavor-dependent long-range neutrino interactions, using DUNE, T2HK, and their combination. DUNE runs for 5 years in ν mode and 5 years in $\bar{\nu}$ mode. T2HK runs for 2.5 years in ν mode and 7.5 years in $\bar{\nu}$ mode. For this plot, we assume that the neutrino mass ordering is normal. Existing limits are from a recent global oscillation fit [1] (2σ), atmospheric neutrinos [2] (90% C.L.), solar and reactor neutrinos [3] (3σ), and non-standard interactions [4–6] (90% C.L.). We show the projected sensitivity (1σ) expected from flavor-composition measurements of high-energy astrophysical neutrinos in IceCube-Gen2 [7]. These limits are for the $L_e - L_\mu$ symmetry; see figure 6 for others. Indirect limits [8] are from black-hole superradiance (90% C.L.) [9], and the weak gravity conjecture [10], assuming a lightest neutrino mass of 0.01 eV. Our projected limits may improve on existing ones, especially for ultra-light mediators of masses below about 10^{-18} eV. See section 4.2 for details, figure 6 for constraints using DUNE or T2HK separately, and figures 7–9 for discovery plots.

This paper is organized as follows. Section 2 introduces lepton-number gauge symmetries, long-range interactions, and their effect on neutrino oscillations. Section 3 overviews DUNE and T2HK, and shows oscillation probabilities and event rates in them. Section 4 shows projected constraints and discovery prospects. Section 5 summarizes and concludes.

2 Flavor-dependent long-range neutrino interactions

2.1 Gauged lepton-number symmetries

In the Standard Model (SM), the baryon number and the lepton numbers, L_e , L_μ , and L_τ , are accidental U(1) global symmetries. Linear combinations of the lepton-number symmetries can be gauged anomaly-free, i.e., without introducing a new fermion or right-handed neutrino (although not simultaneously) [47–50]. To showcase the capabilities of DUNE and T2HK, we explore three such new U(1) gauge symmetries, generated by $L_e - L_\mu$, $L_e - L_\tau$, and $L_\mu - L_\tau$, that introduce new flavor-dependent neutrino-matter interactions; later, we show how they affect neutrino oscillations. (Other combinations of baryon and lepton numbers can also be gauged anomaly-free; see ref. [1].)

Figure 2 shows the Feynman diagrams for neutrino-matter interaction that we consider. For a particular lepton-number symmetry, the corresponding effective Lagrangian is

$$\mathcal{L}_{\text{eff}} = \mathcal{L}_{\text{SM}} + \mathcal{L}_{Z'} + \mathcal{L}_{\text{mix}}. \quad (2.1)$$

The first term describes the SM contribution, mediated by the Z boson, i.e.,

$$\mathcal{L}_{\text{SM}} = \frac{e}{\sin \theta_W \cos \theta_W} Z_\mu \left[-\frac{1}{2} \bar{l}_\alpha \gamma^\mu P_L l_\alpha + \frac{1}{2} \bar{\nu}_\alpha \gamma^\mu P_L \nu_\alpha + \frac{1}{2} \bar{u} \gamma^\mu P_L u - \frac{1}{2} \bar{d} \gamma^\mu P_L d \right], \quad (2.2)$$

where $e/(\sin \theta_W \cos \theta_W) = 0.723$, e is the unit charge, θ_W is the Weinberg angle, ν_α and l_α are a neutrino and charged lepton of flavor $\alpha = e, \mu, \tau$, P_L is the left-handed projection operator, and u and d are up and down quarks. Because the Z boson is heavy, the interaction that it mediates is short-range; in our work, it matters only inside the Earth. (Equation (2.2), and also eq. (2.4) below, assumes that matter is electrically neutral, i.e., that it has equal abundance of electrons and protons [54], which is also what we assume later when computing the new matter potential; see section 2.2.)

The second term in eq. (2.1) describes the interaction between ν_α and l_α mediated by the new $Z'_{\alpha\beta}$ boson [46, 49, 54], i.e., for the $L_\alpha - L_\beta$ symmetry,

$$\mathcal{L}_{Z'} = g'_{\alpha\beta} Z'_\sigma (\bar{l}_\alpha \gamma^\sigma l_\alpha - \bar{l}_\beta \gamma^\sigma l_\beta + \bar{\nu}_\alpha \gamma^\sigma P_L \nu_\alpha - \bar{\nu}_\beta \gamma^\sigma P_L \nu_\beta), \quad (2.3)$$

where $g'_{\alpha\beta}$ is a dimensionless coupling constant. Due to the dearth of naturally occurring muons and tauons with which neutrinos can interact, we neglect this contribution under $L_\mu - L_\tau$ and consider it only under $L_e - L_\mu$ and $L_e - L_\tau$, for which the interaction is sourced by comparatively abundant electrons.

The final term in eq. (2.1) describes the mixing between Z and $Z'_{\alpha\beta}$ [54, 60, 72], which can arise directly or by radiative mixing [73, 74]. In the physical basis, this term is [72] $\mathcal{L}_{ZZ'} \supset (\xi - \sin \theta_W \chi) Z'_\mu Z^\mu$, where χ is the kinetic mixing angle between the two bosons

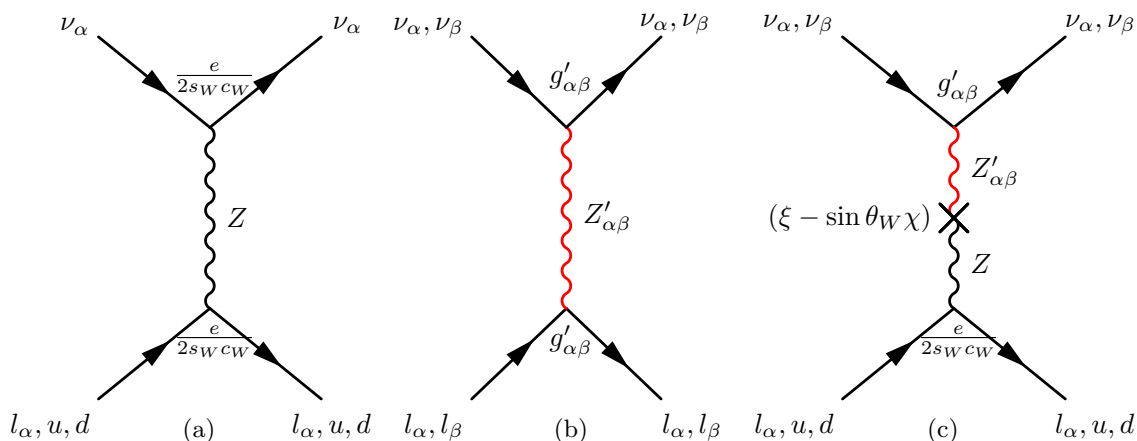


Figure 2. Feynman diagrams for neutrino-matter interactions. Each diagram corresponds to a term in the Lagrangian, eq. (2.1): (a) SM contribution mediated by the Z boson, (b) new contribution from the gauge symmetry $U(1)_{L_\alpha-L_\beta}$, mediated by the new boson $Z'_{\alpha\beta}$, and (c) mixing between Z and $Z'_{\alpha\beta}$. In our analysis, (a) is significant only for neutrinos inside the Earth. For L_e-L_β symmetries, (b) is the only additional contribution sourced by electrons. For $L_\mu-L_\tau$, (c) is instead the only additional contribution sourced by neutrons. See section 2.1 for details.

and ξ is the rotation angle between gauge eigenstates and physical states. This introduces a four-fermion interaction between neutrinos and charged leptons, protons, and neutrons via Z - $Z'_{\alpha\beta}$ mixing, i.e.,

$$\mathcal{L}_{\text{mix}} = -g'_{\alpha\beta}(\xi - \sin \theta_W \chi) \frac{e}{\sin \theta_W \cos \theta_W} J'_\rho J_3^\rho, \quad (2.4)$$

where $J'_\rho = \bar{\nu}_\alpha \gamma_\rho P_L \nu_\alpha - \bar{\nu}_\beta \gamma_\rho P_L \nu_\beta$ and $J_3^\rho = -\frac{1}{2} \bar{e} \gamma^\rho P_L e + \frac{1}{2} \bar{u} \gamma^\rho P_L u - \frac{1}{2} \bar{d} \gamma^\rho P_L d$. However, the contribution of electrons is nullified by that of protons, leaving only neutrons to source the new interaction via mixing. The term $(\xi - \sin \theta_W \chi)$ effectively describes the strength of the Z - $Z'_{\alpha\beta}$ mixing. Its value is unknown, but there are upper limits on it [54, 75, 76]. We do not consider its value independently, but together with $g'_{\alpha\beta}$, as an effective coupling (more on this below). In order to showcase the effect of mixing, we include \mathcal{L}_{mix} only under $L_\mu - L_\tau$.

In summary, under $L_e - L_\mu$ and $L_e - L_\tau$, the new interactions are described by $\mathcal{L}_{Z'}$, and are sourced by electrons only, whereas under $L_\mu - L_\tau$, the new interactions are described by \mathcal{L}_{mix} , and are sourced by neutrons only. In all cases, in addition, standard neutrino-electron interactions, described by \mathcal{L}_{SM} , are active only inside the Earth.

2.2 Long-range matter potential

The above interactions induce flavor-dependent Yukawa potentials, sourced by electrons and neutrons, that affect the mixing of neutrinos [7, 8, 46, 48–50]. Under $L_e - L_\beta$ ($\beta = \mu, \tau$), a neutrino located at a distance d from a collection of N_e electrons experiences a potential

$$V_{e\beta} = G_{\alpha\beta}^{\prime 2} \frac{N_e}{4\pi d} e^{-m'_{e\beta} d}, \quad (2.5)$$

where $m'_{e\beta}$ is the mass of the mediating $Z'_{e\beta}$ boson. Under $L_\mu - L_\tau$, a neutrino located at a distance d from a collection of N_n neutrons experiences a potential

$$V_{\mu\tau} = G'^2_{\alpha\beta} \frac{e}{\sin\theta_W \cos\theta_W} \frac{N_n}{4\pi d} e^{-m'_{\mu\tau}d}, \quad (2.6)$$

where $m'_{\mu\tau}$ is the mass of the mediating $Z'_{\mu\tau}$ boson. In eqs. (2.5) and (2.6), the effective coupling strength is

$$G'_{\alpha\beta} = \begin{cases} g'_{e\mu} & , \text{ for } \alpha, \beta = e, \mu \\ g'_{e\tau} & , \text{ for } \alpha, \beta = e, \tau \\ \sqrt{g'_{\mu\tau}(\xi - \sin\theta_W\chi)} & , \text{ for } \alpha, \beta = \mu, \tau \end{cases}. \quad (2.7)$$

At distances longer than the interaction range of $1/m'_{\alpha\beta}$, the potential is suppressed due to the mediator mass. Like ref. [7], we explore light mediators with $m'_{\alpha\beta} = 10^{-35} - 10^{-10}$ eV, corresponding to interaction ranges from 10^3 Gpc — larger than the observable Universe — to hundreds of meters; see figure 1.

We adopt the methods introduced in ref. [7] to compute the total potential sourced by nearby and faraway electrons and neutrons in the Earth (\oplus), Moon (\mathcal{C}), Sun (\odot), Milky Way (MW), and by the cosmological distribution of matter (cos) in the local Universe, i.e.,

$$V_{\alpha\beta} = V_{\alpha\beta}^\oplus + V_{\alpha\beta}^{\mathcal{C}} + V_{\alpha\beta}^\odot + V_{\alpha\beta}^{\text{MW}} + V_{\alpha\beta}^{\text{cos}}. \quad (2.8)$$

The specific value of $m'_{\alpha\beta}$ determines the relative size of the contributions of the above sources to the total potential. We do not compute the changing potential along the underground trajectories of the neutrinos from source to detector inside the Earth; see ref. [1] for such treatment. Instead, like ref. [7], we compute the average potential experienced by the neutrinos at their point of detection. This approximation is especially valid for mediators lighter than about 10^{-14} eV, for which the interaction range is longer than the radius of the Earth (see figure 1), and so all of the electrons and neutrons on Earth contribute to the potential experienced by a neutrino regardless of its position along its trajectory. Below 10^{-14} eV is also where we place novel projected limits.

We assume that the matter that sources the potential is electrically neutral, so that the number of electrons and protons is the same, and isoscalar, so that the number of electrons and neutrons is the same, except for the Sun [54] and for the cosmological distribution of matter [77–79]. We treat the Moon ($N_{e,\mathcal{C}} = N_{n,\mathcal{C}} \sim 5 \cdot 10^{49}$) and the Sun ($N_{e,\odot} \sim 10^{57}$, $N_{n,\odot} = N_{e,\odot}/4$) as point sources of electrons and neutrons, and the Earth ($N_{e,\oplus} \approx N_{n,\oplus} \sim 4 \times 10^{51}$), the Milky Way ($N_{e,\text{MW}} \approx N_{n,\text{MW}} \sim 10^{67}$), and the cosmological matter ($N_{e,\text{cos}} \sim 10^{79}$, $N_{n,\text{cos}} \sim 10^{78}$) as continuous distributions. We defer to ref. [7] for a detailed calculation of eq. (2.8), but adopt two differences introduced by ref. [80]. First, unlike ref. [7], which studied extragalactic neutrinos and so averaged the contribution of cosmological matter over redshift, here we consider $V_{\alpha\beta}^{\text{cos}}$ to be only the contribution from the local Universe, i.e., we evaluate eq. (A8) in ref. [7] at redshift $z = 0$. Second, unlike ref. [7], which only computed the potential sourced by electrons under $L_e - L_\mu$ and $L_e - L_\tau$, here we compute also the potential sourced by neutrons under $L_\mu - L_\tau$.

2.3 Neutrino oscillation probabilities under long-range interactions

We consider mixing between the three active neutrinos, ν_e , ν_μ , and ν_τ . Under the $L_\alpha - L_\beta$ symmetry, the Hamiltonian that drives neutrino propagation, in the flavor basis, is

$$\mathbf{H} = \mathbf{H}_{\text{vac}} + \mathbf{V}_{\text{mat}} + \mathbf{V}_{\alpha\beta}. \quad (2.9)$$

The first two terms on the right-hand side induce standard oscillations, including SM matter effects; the third one, oscillations due to the new interactions.

In vacuum, oscillations are driven by

$$\mathbf{H}_{\text{vac}} = \frac{1}{2E} \mathbf{U} \text{diag}(0, \Delta m_{21}^2, \Delta m_{31}^2) \mathbf{U}^\dagger, \quad (2.10)$$

where E is the neutrino energy, $\Delta m_{ij}^2 \equiv m_i^2 - m_j^2$ are the mass-squared splittings between neutrino mass eigenstates, and \mathbf{U} is the Pontecorvo-Maki-Nakagawa-Sakata (PMNS) mixing matrix, parametrized [81] in terms of the mixing angles θ_{12} , θ_{23} , and θ_{13} , and the CP-violating phase, δ_{CP} . In the main text, we show results assuming normal neutrino mass ordering (NMO), where $m_1 < m_2 < m_3$; table 1 shows the values of the mixing parameters that we use, taken from ref. [82]. Appendix C contains results obtained under the inverted mass ordering (IMO), where $m_3 < m_2 < m_1$.

In eq. (2.9), the contribution of SM coherent forward scattering on electrons, mediated by the W boson, is

$$\mathbf{V}_{\text{mat}} = \text{diag}(V_{\text{CC}}, 0, 0), \quad (2.11)$$

where $V_{\text{CC}} = \sqrt{2}G_F n_e \simeq 7.6Y_e[\rho/(10^{14} \text{ g cm}^{-3})] \text{ eV}$ is the charged-current neutrino-electron interaction potential, G_F is the Fermi constant, n_e is the electron number density, $Y_e \equiv n_e/(n_p + n_n)$ is the electron fraction, i.e., its abundance relative to that of protons and neutrons, n_p and n_n , and ρ is the matter density. In our work, this contribution is relevant only inside Earth, where matter densities are high. We take ρ to be the average density of underground matter along the trajectory from source to detector, calculated using the Preliminary Reference Earth Model [83]: 2.848 g cm^{-3} for DUNE and 2.8 g cm^{-3} for T2HK. The potential above is for neutrinos; for antineutrinos, it flips sign, i.e., $\mathbf{V}_{\text{mat}} \rightarrow -\mathbf{V}_{\text{mat}}$.

Finally, in eq. (2.9) the contribution from the new matter interaction is

$$\mathbf{V}_{\alpha\beta} = \begin{cases} \text{diag}(V_{e\mu}, -V_{e\mu}, 0), & \text{for } \alpha, \beta = e, \mu \\ \text{diag}(V_{e\tau}, 0, -V_{e\tau}), & \text{for } \alpha, \beta = e, \tau \\ \text{diag}(0, V_{\mu\tau}, -V_{\mu\tau}), & \text{for } \alpha, \beta = \mu, \tau \end{cases}, \quad (2.12)$$

where the potential, $V_{\alpha\beta}$, eq. (2.8), depends on the mediator mass, $m'_{\alpha\beta}$, and coupling, $G'_{\alpha\beta}$. The potential above is for neutrinos; for antineutrinos, it flips sign, i.e., $\mathbf{V}_{\alpha\beta} \rightarrow -\mathbf{V}_{\alpha\beta}$.

The $\nu_\alpha \rightarrow \nu_\beta$ transition probability associated to the Hamiltonian, eq. (2.9), is

$$P_{\nu_\alpha \rightarrow \nu_\beta} = \left| \sum_{i=1}^3 U'_{\alpha i} \exp\left(\frac{\Delta \tilde{m}_{i1}^2 L}{2E}\right) U'_{\beta i}{}^* \right|^2, \quad (2.13)$$

where L is the distance traveled by the neutrino from production to detection, $\Delta \tilde{m}_{ij}^2 \equiv \tilde{m}_i^2 - \tilde{m}_j^2$, with $\tilde{m}_i^2/2E$ the eigenvalues of the Hamiltonian, modified from those of \mathbf{H}_{vac} by matter

effects, and \mathbf{U}' is the unitary matrix that diagonalizes the Hamiltonian. We parametrize \mathbf{U}' with the same shape as the PMNS matrix, but evaluated at mixing parameters θ_{12}^m , θ_{23}^m , θ_{13}^m , and δ_{CP}^m modified by matter effects. In our work, we compute the oscillation probability, eq. (2.13), exactly and numerically to arbitrary precision; see refs. [56, 58, 84–90] for approximate analytical solutions.

For the new matter interactions to affect the oscillation probability, the new matter potential must be at least comparable to the standard contributions in eq. (2.9), i.e., in vacuum, $V_{\alpha\beta} \gtrsim (\Delta m_{31}^2/2E)$ [inside the Earth, this is instead $V_{\alpha\beta} \gtrsim \max(\Delta m_{31}^2/2E, V_{\text{CC}})$]. In DUNE and T2HK, where the first oscillation maxima occur at 2.6 GeV and 0.6 GeV, respectively, this implies that they become important for $V_{\alpha\beta} \gtrsim 10^{-13}$ eV. This sets the scale of the potential to which our analysis is sensitive. Later, in section 3.2, we show how the new interactions affect the probabilities in DUNE and T2HK.

2.4 Existing limits

Figure 1 (also figure 6) shows existing limits on flavor-dependent long-range neutrino interactions. Below, we summarize them. We focus on light mediators; the complementary case for heavy mediators was first studied in refs. [46, 48–50, 91].

Pioneering studies in refs. [2] and [3] identified the potential of neutrino oscillations to test new long-range interactions, possibly more stringently than gravitational probes. They focused on interactions with a range equal to the Earth-Sun distance [though ignoring the Yukawa suppression in eq. (2.5)] and sourced by solar electrons. Reference [2] used Super-Kamiokande atmospheric neutrino data to find $g'_{e\mu} < 8.32 \times 10^{-26}$ and $g'_{e\tau} < 8.97 \times 10^{-26}$, at 90% confidence level (C.L.) Reference [3] used solar and reactor neutrino data from KamLAND to find $g'_{e\mu} < 2.06 \times 10^{-26}$ and $g'_{e\tau} < 1.77 \times 10^{-26}$, at 3σ , assuming $\theta_{13} = 0^\circ$.

Reference [54] studied the effect of the $L_\mu - L_\tau$ symmetry via kinetic mixing (see section 2.1) on ν_μ in the long-baseline experiment MINOS. By comparing the potential $V_{\mu\tau}$ sourced by a neutron in the Sun to the fifth-force gravitational potential sourced by it, and applying upper limits on the strength of the latter from torsion-balance experiments [75, 76], ref. [54] set an upper limit on the mixing strength of $(\xi - \sin\theta_W\chi) < 5 \times 10^{-24}$ at 95% C.L. for a long-range interaction with range equal to the Earth-Sun distance. (This is the limit that we saturate when computing the $V_{\mu\tau}$ potential, eq. (2.6); see section 2.1.) This translates into an upper limit of $g'_{\mu\tau} \leq 2.51 \times 10^{-26}$. For an interaction with a range of the size of the Earth, the upper limit degrades to $g'_{\mu\tau} \leq 10^{-24}$.

Reference [8] showed that upper limits on the coefficients that parametrize the strength of non-standard neutrino interactions (NSI) can be translated into upper limits on the coupling strength of flavor-dependent long-range interactions. Figure 1 shows the resulting limits, based on the NSI limits from refs. [4–6].

Recently, ref. [1] performed a global oscillation analysis of new U(1) symmetries, including $L_e - L_\mu$ and $L_e - L_\tau$, by using the same experimental data sets used in NuFIT 5.0 [92, 93]. Unlike our analysis, ref. [1] computed the changing long-range matter potential due to underground matter in the Earth along the trajectory of the neutrinos. Their procedure is more detailed than ours for mediators lighter than 10^{-14} eV. However, they explore masses only as low as 10^{-18} eV, i.e., an interaction range of 1 A.U.

Reference [7] first showed that the flavor composition of TeV–PeV astrophysical neutrinos, i.e., the relative number of ν_e , ν_μ , and ν_τ , can be used to probe long-range interactions under $L_e - L_\mu$ and $L_e - L_\tau$ sourced by the same collections of nearby and distant electrons that we consider here. Reference [80] refined the statistical methods and included also $L_\mu - L_\tau$. The main effect is that, if the potential sourced by electrons or neutrons were to be dominant, oscillations would turn off, and the flavor composition emitted by the astrophysical sources and received at Earth would be the same; see also ref. [94]. Figure 1 shows the projected upper limits obtained in ref. [7] based on estimates of flavor-composition measurements in the envisioned IceCube-Gen2 neutrino telescope [95].

Finally, following ref. [8], figure 1 includes two indirect limits. First, ref. [9] excluded three mediator mass windows (“Black-hole superradiance”) by considering the superradiant growth rate of a gravitationally bound accumulation of light vector bosons around selected stellar-mass and supermassive black holes. Second, ref. [10] placed a tentative lower limit on the coupling (“Weak gravity conjecture”) by studying low-energy effective theories that contain gravity and U(1) gauge fields where at least one particle charged under U(1) is essential for gravity to be the weakest force.

In figure 1, we show existing limits as they were published in their original references. Hence, they do not extend to mediators lighter than 10^{-14} – 10^{-20} eV, depending on the limit (except for the proof-of-principle sensitivity based on projected IceCube-Gen2 measurements of the flavor composition [7]). These limits could be recomputed and extended to span lighter mediators, using the same long-range matter potential that we have used, eq. (2.8), though doing so lies beyond the scope of this work.

3 Long-range interactions in DUNE and T2HK

3.1 Overview of the experiments

Long-baseline neutrino experiments are powerful probes of neutrino oscillations [96–99]. Owing to baselines of hundreds of kilometers and well-characterized GeV-scale neutrino beams, they can probe matter effects in oscillations, CP violation, neutrino mass ordering, and a large number of possible new neutrino physics [96–101]. Today, long-baseline experiments T2K [102] and NO ν A [103] contribute high-precision data to global oscillation fits [82, 92]. In the coming decade, next-generation experiments DUNE [17, 104–108], T2HK [18, 19], and the European Spallation Source neutrino Super Beam (ESS ν SB) [109, 110], currently under construction, will take this further [96–101].

In our forecasts, we focus on DUNE and T2HK. Below, we overview their features. For each one, we compute appearance and disappearance oscillation probabilities and event rates in neutrino (ν) and antineutrino ($\bar{\nu}$) beam modes:

Appearance, ν mode: This is sensitive mainly to $\nu_\mu \rightarrow \nu_e$ transitions. The beam works in neutrino mode, and the detector targets ν_e -initiated events.

Appearance, $\bar{\nu}$ mode: This is sensitive mainly to $\bar{\nu}_\mu \rightarrow \bar{\nu}_e$ transitions. The beam works in antineutrino mode, and the detector targets $\bar{\nu}_e$ -initiated events.

	Standard mixing parameters (NMO)					
	$\sin^2 \theta_{12}$	$\sin^2 \theta_{23}$	$\sin^2 \theta_{13}$	$\frac{\Delta m_{31}^2}{10^{-3} \text{eV}^2}$	$\frac{\Delta m_{21}^2}{10^{-5} \text{eV}^2}$	$\delta_{\text{CP}} (^\circ)$
Benchmark	0.303	0.455	0.0223	2.522	7.36	223
Status in fits	Fixed	Minimized	Fixed	Minimized	Fixed	Minimized
Range	–	[0.4, 0.6]	–	[2.438, 2.602]	–	[139, 355]

Table 1. *Values of the standard mixing parameters used in our analysis.* We assume normal neutrino mass ordering (NMO) in the main text. The benchmark values are the best-fit values from ref. [82]. For each parameter over which we minimize our test statistic (see section 4.1), the minimum is searched for within the range shown, which is the 3σ allowed range from ref. [82]. We assume no correlation between the parameters. Table 5 shows the parameter ranges that we use in appendix C to obtain results under the inverted mass ordering (IMO) instead.

Disappearance, ν mode: This is sensitive mainly to $\nu_\mu \rightarrow \nu_\mu$ survival. The beam works in neutrino mode, and the detector targets ν_μ -initiated events.

Disappearance, $\bar{\nu}$ mode: This is sensitive mainly to $\bar{\nu}_\mu \rightarrow \bar{\nu}_\mu$ survival. The beam works in antineutrino mode, and the detector targets $\bar{\nu}_\mu$ -initiated events.

DUNE will also detect ν_τ with energies larger than 3.4 GeV via their charged-current interactions, which allows for interesting physics opportunities [111–115]. However, in our analysis, we focus on ν_e appearance only and treat ν_τ appearance as background; see below.

Table 1 shows the values and allowed ranges of the mixing parameters that we use in our analysis, taken from the global oscillation fit of ref. [82]. In the main text, we show results assuming that the true neutrino mass ordering is normal, since there is currently weak preference for it [82, 92, 93, 116]. However, as part of our statistical analysis in section 4, we report sensitivity after minimizing over the mass ordering. Appendix C contains results assuming instead that the true mass ordering is inverted.

3.1.1 DUNE

DUNE will consist of a near detector, about 600 m downstream of the neutrino production point on the Fermilab site, and a far detector, 1285 km away and about 1.5 km underground, in the Sanford Underground Research Facility in South Dakota [117]. The near detector will monitor and characterize the neutrino beam (though it has physics capabilities itself, too [118, 119]). We focus on the far detector since it offers prime sensitivity to neutrino oscillations. It is a state-of-the-art liquid-argon time projection chamber with a net volume of 40 kton; to generate our results, we consider single-phase detection only [107]. Neutrino detection is via charged-current neutrino-argon interaction. Detector deployment will be phased [108], but in our simulations we consider only the final, total detector volume.

DUNE will use the Long Baseline Neutrino Facility (LBNF) neutrino beam produced at Fermilab. There, the Main Injector of the LBNF fires a 1.2-MW beam of protons of 120 GeV onto a graphite target, producing charged mesons that decay in flight to neutrinos. The resulting neutrino flux is wide-band, ranges from a few hundreds of MeV to a few tens

of GeV, and is expected to peak at 2.5 GeV, with most neutrinos in the 1–5 GeV range. By changing the polarity of the focusing horns [120, 121], the experiment can run in neutrino or antineutrino mode. Following the DUNE Technical Design Report [107], we adopt a run time of 5 years in neutrino mode and 5 years in antineutrino mode. This amounts to 1.1×10^{21} protons-on-target per year and a net exposure of 480 kton MW year. To produce our results, we use the DUNE simulation configuration from ref. [17].

3.1.2 T2HK

T2HK will consist of near detectors, about 280 m downstream from the neutrino production point at the Japan Proton Accelerator Research Complex (JPARC), and a far detector, 295 km away and about 1.7 km underground, in the Tochibora mines of Japan, 8 km from Super-Kamiokande [45]. Like in DUNE, the near detectors will monitor and characterize the neutrino beam, and we focus on the far detector. It will be a tank filled with purified water, with a net volume of 187 kton, whose internal wall is lined with photomultipliers (PMTs). Neutrino detection is via quasielastic charged-current scattering (QECC), i.e., $\nu_l + n \rightarrow p + l^-$ and $\bar{\nu}_l + p \rightarrow n + l^+$ ($l = e, \mu, \tau$), and via charged-current deep inelastic scattering (DIS), i.e., $\nu_l + N \rightarrow l^- + X$ and $\bar{\nu}_l + N \rightarrow l^+ + X$ ($l = e, \mu$), where X represents final-state hadrons (ν_τ DIS is suppressed due to the large tauon mass). Electrons emit gamma rays by bremsstrahlung and e^+e^- annihilation, which register as a fuzzy ring on the PMTs. Muons emit Cherenkov light, which registers as a sharply defined ring.

Like its predecessor, T2K (Tokai-to-Kamioka) [102], T2HK will use the 2.5° -off-axis JPARC neutrino beam [122]. To produce it, JPARC fires a 1.3-MW beam of protons of 30 GeV onto a graphite target. The resulting neutrino flux is narrow-band, ranges from a few MeV to a few GeV, and is expected to peak at 600 MeV, with most neutrinos in the 100–3000 MeV range. As in DUNE, by changing the polarity of the focusing horns, T2HK can run in neutrino or antineutrino mode [123]. Following ref. [18], we adopt a run time of 2.5 years in neutrino mode and 7.5 years in antineutrino mode, in accordance with the default 1:3 ratio planned for them. This amounts to 2.7×10^{22} protons-on-target per year and a net exposure of 2431 kton MW year. To produce our results, we match the binned event spectra that we generate under standard oscillations with those of ref. [18].

3.2 Oscillation probabilities

Appendix A, especially figure 10 therein, shows in detail the effects of long-range interactions on the modified mixing parameters θ_{12}^m , θ_{23}^m , and θ_{13}^m ; here, we summarize them. Differences in their behavior under the different symmetries stem from differences in the flavor structure of the new matter potential, $\mathbf{V}_{\alpha\beta}$ in eq. (2.9).

The solar angle in matter rapidly approximates its maximum value of $\theta_{12}^m = 90^\circ$ already at a few GeV, for all symmetries. (We use this later, in section 4.1, to justify why we neglect the effect on our forecasts of the uncertainty in its value in vacuum, θ_{12} .) For DUNE and T2HK, the mixing angles that drive the probabilities are the atmospheric angle, θ_{23}^m , and the reactor angle, θ_{13}^m . Assuming $\theta_{12}^m = 90^\circ$, ref. [58] showed that the transition probabilities for $\nu_\mu \rightarrow \nu_e$ and $\bar{\nu}_\mu \rightarrow \bar{\nu}_e$ are $\propto \sin^2 \theta_{23}^m \sin^2 \theta_{13}^m$ and the survival probabilities for $\nu_\mu \rightarrow \nu_\mu$ and $\bar{\nu}_\mu \rightarrow \bar{\nu}_\mu$ are $\propto \sin^2 2\theta_{23}^m$, with a more nuanced dependence on θ_{13}^m . The deviation

of θ_{23}^m relative to θ_{23} grows with energy, though there are differences depending on which symmetry is active: θ_{23}^m grows under $L_e - L_\tau$ and $L_\mu - L_\tau$, and shrinks under $L_e - L_\mu$. The reactor angle in matter, θ_{13}^m , grows appreciably with energy under $L_e - L_\mu$ and $L_e - L_\tau$, and falls to about 0° under $L_\mu - L_\tau$.

Figure 3 shows the oscillation probabilities, eq. (2.13), computed under the three symmetries in each of the four detection channels listed in section 3.1, for DUNE and T2HK. To illustrate the effects of long-range interactions, we pick a relatively high value of the potential, $V_{\alpha\beta} = 1.3 \times 10^{-13}$ eV; later, when producing our results, we vary this value. Via eq. (2.8), multiple combinations of $m'_{\alpha\beta}$ and $G'_{\alpha\beta}$ can yield this value of the potential, or any other. Because the baseline for DUNE is longer than for T2HK, the effects of long-range interactions with underground matter on the probabilities in the former are more prominent than in the latter [90]. The effects are more clearly visible in the transition probabilities: the oscillation maxima shift to lower energies, due to a change in the effective mass-splitting $\Delta m_{31,m}^2$, in agreement with ref. [56], and the oscillation amplitudes grow, especially after the first maximum. The effects are more prominent under $L_e - L_\tau$ because θ_{23}^m and θ_{13}^m are enhanced, whereas under $L_e - L_\mu$ and $L_\mu - L_\tau$ only one of them is; see appendix A for details. Naturally, for weaker potentials, the above effects are lessened.

3.3 Event rates

We compute event rates in DUNE and T2HK using GLOBES [124, 125], extended with the SNU matrix-diagonalization library [126, 127], by modeling their technical design specifications [17, 19] of efficiency, operation times, and backgrounds. Because we are interested in assessing the mean sensitivity of the experiments (section 4.1), we compute only mean event rates and do not generate event spectra that include fluctuations from the mean rates. We bin event rates in reconstructed energy, E_{rec} , built from the detected secondaries born in neutrino interactions. In both experiments, because the far detectors cannot distinguish between neutrinos and antineutrinos, there is irreducible contamination from “wrong-sign” events; we add it to the signal.

DUNE. We consider events with E_{rec} in the range 0–110 GeV, with 64 bins within 0–8 GeV, each 0.125 GeV wide, and 16 bins within 8–110 GeV, of varying widths. In the appearance channel, the signal is due to the charged-current (CC) interactions of ν_e , in neutrino mode, and of $\bar{\nu}_e$, in antineutrino mode. The background consists of (i) the CC interactions of “intrinsic” ν_e and $\bar{\nu}_e$, i.e., those created as such that survive the flight to the detector (from $\nu_e \rightarrow \nu_e$ and $\bar{\nu}_e \rightarrow \bar{\nu}_e$); (ii) the CC interactions of ν_μ and $\bar{\nu}_\mu$ whose final-state muons are misidentified as electrons (from $\nu_\mu \rightarrow \nu_\mu$ and $\bar{\nu}_\mu \rightarrow \bar{\nu}_\mu$); (iii) the CC interactions of ν_τ and $\bar{\nu}_\tau$ (from $\nu_\mu \rightarrow \nu_\tau$ and $\bar{\nu}_\mu \rightarrow \bar{\nu}_\tau$); and (iv) the neutral-current (NC) interactions of neutrinos of all flavors. In the disappearance channel, the signal is due to the CC interactions of ν_μ , in neutrino mode, and of $\bar{\nu}_\mu$, in antineutrino mode. The background consists of (i) the CC interactions of ν_τ and $\bar{\nu}_\tau$ (from $\nu_\mu \rightarrow \nu_\tau$ and $\bar{\nu}_\mu \rightarrow \bar{\nu}_\tau$); and (ii) the NC interactions of neutrinos of all flavors.

T2HK. We consider events with E_{rec} in the range 0.1–3 GeV, with 29 bins, each 0.1 GeV wide. In the appearance channel, the signal is due to the CC interactions of ν_e , in neutrino

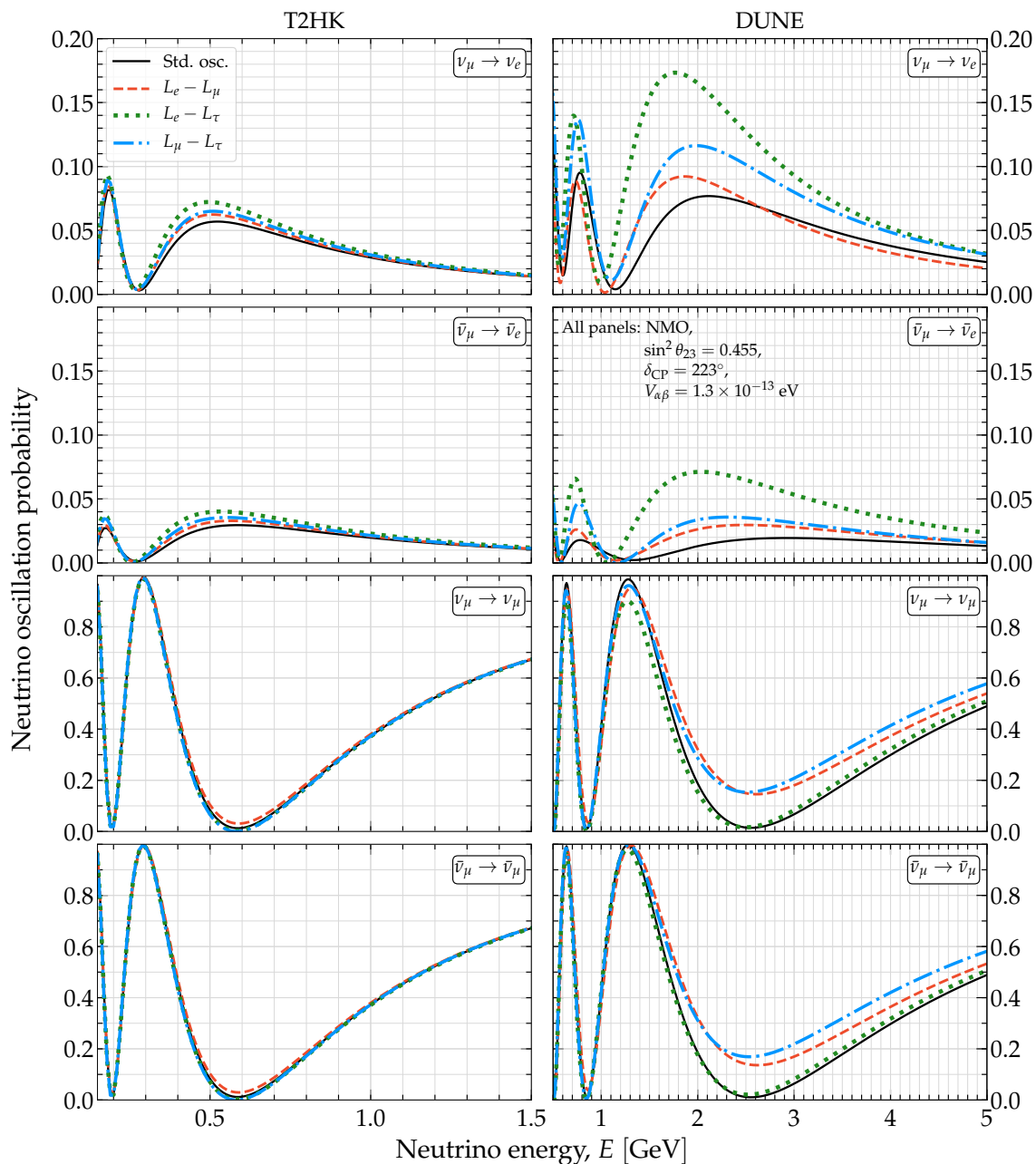


Figure 3. Neutrino oscillation probabilities for T2HK (left column) and DUNE (right column) under flavor-dependent long-range neutrino interactions. The interactions are induced by the lepton-number symmetry $L_e - L_\mu$, $L_e - L_\tau$, or $L_\mu - L_\tau$. For this figure, we fix the long-range potential to $V_{\alpha\beta} = 1.3 \times 10^{-13}$ eV as illustration, and the standard mixing parameters to their benchmark values from table 1. See section 3.2 for details.

mode, and of $\bar{\nu}_e$, in antineutrino mode. The background consists of (i) the CC interactions of intrinsic ν_e and $\bar{\nu}_e$ (from $\nu_e \rightarrow \nu_e$ and $\bar{\nu}_e \rightarrow \bar{\nu}_e$); (ii) the CC interactions of ν_μ and $\bar{\nu}_\mu$ whose final-state muons produce fuzzy Cherenkov rings; and (iii) the NC interactions of neutrinos of all flavors. In the disappearance channel, the signal is due to the CC interactions of ν_μ , in neutrino mode, and of $\bar{\nu}_\mu$, in antineutrino mode. The background consists of (i) the CC interactions of intrinsic ν_e and $\bar{\nu}_e$ (from $\nu_e \rightarrow \nu_e$ and $\bar{\nu}_e \rightarrow \bar{\nu}_e$); and (ii) the NC interactions of neutrinos of all flavors.

Figure 4 shows the mean event-rate spectra under long-range interactions for each detection channel in DUNE and T2HK, including all the above backgrounds, and computed using the same illustrative value of the long-range potential $V_{\alpha\beta}$ as in figure 3. The event rates in T2HK are higher than in DUNE due to its larger size. The shapes of the event spectra in figure 4 reflect those of the oscillation probabilities in figure 3. Long-range interactions affect each detection channel differently, but there are common features among them. Broadly stated, in the appearance channels, they enhance the event rates relative to the standard-oscillations rates (with the exception of $L_e - L_\mu$ in neutrino mode for DUNE). For DUNE, additionally, they slightly shift the event rates to lower energies, reflecting the shift in the oscillation maxima. In the disappearance channels, the effect of long-range interactions is more nuanced; the event rate is enhanced or reduced depending on the symmetry and the energy. The above features in the event spectra hold for other values of the potential, though, naturally, their prominence varies depending on the value.

Table 2 shows the mean expected number of signal and background events for each detection channel, assuming standard oscillations. In all channels, the signal is dominant. In T2HK, unlike DUNE, neutrino and antineutrino event rates are comparable, due to the 1:3 ratio between run times in neutrino and antineutrino modes that compensates for the smaller antineutrino cross sections. In DUNE, neutrino event rates are higher than T2HK due to its longer run time in neutrino mode. These general features of the event rates hold also in the presence of long-range interactions.

Below, we show how the above features grant DUNE and T2HK the capability to probe long-range interactions, and how they organically complement each other.

4 Projected constraints and discovery potential

4.1 Statistical methods

We forecast the capability of DUNE and T2HK to probe long-range interactions that stems from the modification of the oscillation probabilities (section 3.2), based on the detailed computation of event rates outlined above (section 3.3). Our forecasts are two-fold: we forecast *constraints* on long-range interactions — on the long-range matter potential and ultimately on the mediator mass and coupling — assuming that no evidence for them is found, and we forecast prospects of *discovering* them and measuring their parameter values.

We study each symmetry, $L_e - L_\mu$, $L_e - L_\tau$, and $L_\mu - L_\tau$, separately. For a given symmetry, we generate two sets of event spectra, including signal plus backgrounds, for each of the four detection channels of T2HK and DUNE (section 3.3): a “true” spectrum, which we take to be the observed spectrum, and a set of “test” spectra, generated for

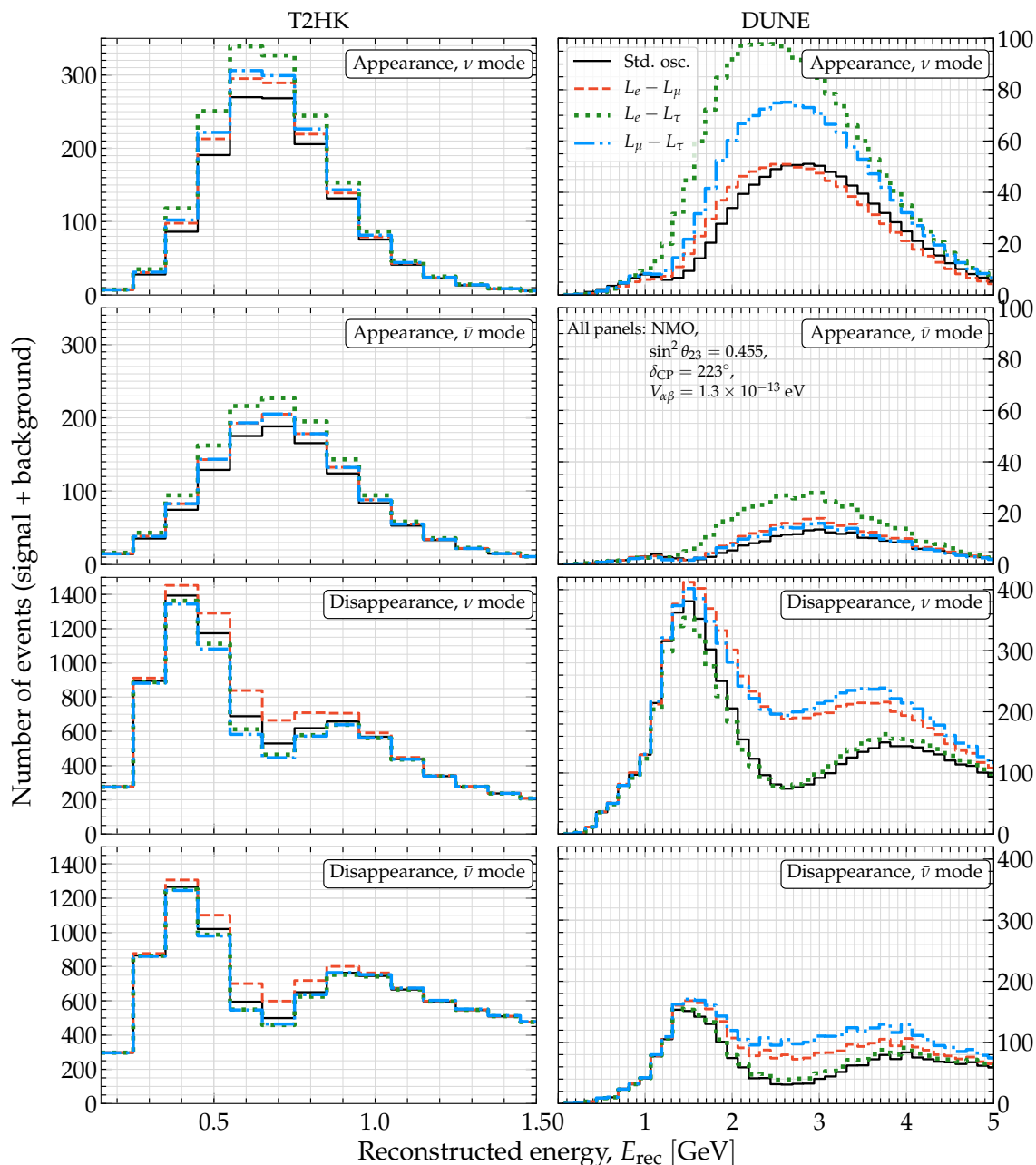


Figure 4. Expected mean number of detected events in T2HK (left column) and DUNE (right column) under flavor-dependent long-range neutrino interactions. The interactions are induced by the symmetry $L_e - L_\mu$, $L_e - L_\tau$, or $L_\mu - L_\tau$. For T2HK, we use 2.5 years in ν mode and 7.5 years in $\bar{\nu}$ mode. For DUNE, we use 5 years in ν mode and 5 years in $\bar{\nu}$ mode. For this figure, we fix the long-range potential to $V_{\alpha\beta} = 1.3 \times 10^{-13}$ eV as illustration, and the standard mixing parameters to their benchmark values from table 1. See section 3.3 for details.

Detector		Mean number of events (standard oscillations, NMO)			
		Appearance		Disappearance	
		ν mode	$\bar{\nu}$ mode	ν mode	$\bar{\nu}$ mode
DUNE	Signal	1390	387	15574	8975
	Bkg.	690	457	347	210
T2HK	Signal	1374	1166	10083	13905
	Bkg.	802	991	1686	1769

Table 2. Mean number of signal and background events, summed over all background channels, expected in DUNE and T2HK after their full run times. For this table, whose aim is illustrative only, we assume standard oscillations and normal mass ordering (NMO). DUNE runs for 5 years in ν mode and 5 years in $\bar{\nu}$ mode. T2HK runs for 2.5 years in ν mode and 7.5 years in $\bar{\nu}$ mode. To compute the rates in this table, we fix the values of the standard mixing parameters to their benchmark values from ref. [82]; see table 1. In the main text, to produce results, we also compute event rates in the presence of the new long-range neutrino interactions (not shown in this table). In those cases, the relative sizes of the event rates in the different detection channels are roughly as in this table. See section 3.3 for details.

test values of the parameters, that we compare against it. When forecasting constraints, in section 4.2, we compute the true spectrum fixing the true value of the potential to be $V_{\alpha\beta}^{\text{true}} = 0$, which corresponds to standard oscillations. When forecasting discovery prospects, in section 4.3, we compute the true spectrum fixing $V_{\alpha\beta}^{\text{true}}$ to a specific nonzero choice. We expand on this below.

To compare true and test event spectra, we follow refs. [128–130] and adopt a Poissonian χ^2 function. For each experiment $e = \{\text{T2HK, DUNE}\}$, and for each detection channel $c = \{\text{app } \nu, \text{app } \bar{\nu}, \text{disapp } \nu, \text{disapp } \bar{\nu}\}$, this is

$$\chi_{e,c}^2(V_{\alpha\beta}, \boldsymbol{\theta}, o) = \min_{\{\xi_s, \{\xi_{b,c,k}\}\}} \left\{ 2 \sum_{i=1}^{N_e} \left[N_{e,c,i}^{\text{test}}(V_{\alpha\beta}, \boldsymbol{\theta}, o, \xi_s, \{\xi_{b,c,k}\}) - N_{e,c,i}^{\text{true}} \left(1 + \ln \frac{N_{e,c,i}^{\text{test}}(V_{\alpha\beta}, \boldsymbol{\theta}, o, \xi_s, \{\xi_{b,c,k}\})}{N_{e,c,i}^{\text{true}}} \right) \right] + \xi_s^2 + \sum_k \xi_{b,c,k}^2 \right\}, \quad (4.1)$$

where $N_{e,c,i}^{\text{true}}$ and $N_{e,c,i}^{\text{test}}$ are the true and test event rates in the i -th bin of E_{rec} , N_e is the number of bins of E_{rec} (section 3.3), $\boldsymbol{\theta} \equiv \{\sin^2 \theta_{23}, \delta_{\text{CP}}, |\Delta m_{31}^2|\}$ are the test values of the most relevant mixing parameters (more on this later), $o = \{\text{NMO, IMO}\}$ is the test mass ordering, and ξ_s and $\xi_{b,c,k}$ are, respectively, pull terms for the systematic uncertainties on the signal and the k -th background contribution to detection channel c , from the list of contributions in section 3.3. The pull terms have the same values in neutrino and antineutrino mode, and are uncorrelated with one another. The true number of events is

$$N_{e,c,i}^{\text{true}} = N_{e,c,i}^{s,\text{true}} + N_{e,c,i}^{b,\text{true}}, \quad (4.2)$$

where $N_{e,c,i}^{s,\text{true}}$ and $N_{e,c,i}^{b,\text{true}}$ are, respectively, the number of signal (s) and background (b) events, summed over all channels, computed using the true values of the mixing parameters,

mass ordering, and potential. The test number of events is

$$N_{e,c,i}^{\text{test}}(V_{\alpha\beta}, \boldsymbol{\theta}, o, \xi_s, \{\xi_{b,c,k}\}) = N_{e,c,i}^s(V_{\alpha\beta}, \boldsymbol{\theta}, o)(1 + \pi_{e,c}^s \xi_s) + \sum_k N_{e,c,k,i}^b(\boldsymbol{\theta}, o) \left(1 + \pi_{e,c,k}^b \xi_{b,c,k}\right), \quad (4.3)$$

where $\pi_{e,c}^s$ and $\pi_{e,c,k}^b$ are normalization errors on the signal and background rates, which lie between 2% and 10%; see table 7 in appendix D for their values, taken from refs. [17, 19]. The background rates do not vary significantly upon changing the mass ordering.

For T2HK or DUNE, separately or together, we compute the total χ^2 by adding the contributions of all the detection channels, i.e.,

$$\chi_{\text{DUNE}}^2(V_{\alpha\beta}, \boldsymbol{\theta}, o) = \sum_c \chi_{\text{DUNE},c}^2(V_{\alpha\beta}, \boldsymbol{\theta}, o), \quad (4.4)$$

$$\chi_{\text{T2HK}}^2(V_{\alpha\beta}, \boldsymbol{\theta}, o) = \sum_c \chi_{\text{T2HK},c}^2(V_{\alpha\beta}, \boldsymbol{\theta}, o), \quad (4.5)$$

$$\chi_{\text{DUNE+T2HK}}^2(V_{\alpha\beta}, \boldsymbol{\theta}, o) = \chi_{\text{DUNE}}^2(V_{\alpha\beta}, \boldsymbol{\theta}, o) + \chi_{\text{T2HK}}^2(V_{\alpha\beta}, \boldsymbol{\theta}, o), \quad (4.6)$$

and we take the contributions of different channels to be uncorrelated.

We report sensitivity by comparing the minimum value of the χ^2 function, $\chi_{e,\text{min}}^2$, reached when it is evaluated at the true values of the parameters, $V_{\alpha\beta}^{\text{true}}$, $\boldsymbol{\theta}^{\text{true}}$, and o^{true} , against the value of χ^2 evaluated at test values of the parameters. We treat $\boldsymbol{\theta}$ and o as nuisance parameters and profile over them (more on this below). For instance, for DUNE,

$$\Delta\chi_{\text{DUNE}}^2(V_{\alpha\beta}) = \min_{\{\boldsymbol{\theta}, o\}} \left[\chi_{\text{DUNE}}^2(V_{\alpha\beta}, \boldsymbol{\theta}, o) - \chi_{\text{DUNE},\text{min}}^2 \right], \quad (4.7)$$

and similarly for T2HK and DUNE+T2HK. In the main text, we fix $\boldsymbol{\theta}^{\text{true}}$ to its present-day best-fit value under NMO, from ref. [82] (table 1) and o^{true} also to NMO; we fix them to inverted mass ordering in appendix C. When reporting *constraints* on long-range interactions, we set $V_{\alpha\beta}^{\text{true}} = 0$ and extract from $\Delta\chi_{\text{DUNE}}^2$, $\Delta\chi_{\text{T2HK}}^2$, and $\Delta\chi_{\text{DUNE+T2HK}}^2$ the upper limits on the inferred value of $V_{\alpha\beta}$, for 1 degree of freedom (d.o.f). When reporting *discovery potential*, we fix $V_{\alpha\beta}^{\text{true}}$ to a nonzero illustrative value and report the inferred range of values of $V_{\alpha\beta}$, again for 1 d.o.f. When reporting discovery, we also study the correlation between $V_{\alpha\beta}$ and δ_{CP} or $\sin^2 \theta_{23}$. In those cases, we use instead, respectively,

$$\Delta\chi_{\text{DUNE}}^2(V_{\alpha\beta}, \delta_{\text{CP}}) = \min_{\{\sin^2 \theta_{23}, |\Delta m_{31}^2|, o\}} \left[\chi_{\text{DUNE}}^2(V_{\alpha\beta}, \boldsymbol{\theta}, o) - \chi_{\text{DUNE},\text{min}}^2 \right], \quad (4.8)$$

$$\Delta\chi_{\text{DUNE}}^2(V_{\alpha\beta}, \sin^2 \theta_{23}) = \min_{\{\delta_{\text{CP}}, |\Delta m_{31}^2|, o\}} \left[\chi_{\text{DUNE}}^2(V_{\alpha\beta}, \boldsymbol{\theta}, o) - \chi_{\text{DUNE},\text{min}}^2 \right], \quad (4.9)$$

and similarly for T2HK and DUNE + T2HK, and we show allowed regions for 2 d.o.f. After placing bounds on $V_{\alpha\beta}$, we translate them into bounds on $G'_{\alpha\beta}$ for varying $m'_{\alpha\beta}$ by means of the definition of the long-range matter potential, eq. (2.8).

When profiling, we minimize the $\Delta\chi^2$ functions above with respect to $\sin^2 \theta_{23}$, δ_{CP} , and $|\Delta m_{31}^2|$ by varying them within their 3σ allowed ranges from ref. [82]; see table 1. We do not include correlations between them, since these are expected to weaken in coming years (see, e.g., ref. [131]), nor do we include pull terms on the mixing parameters in the

test-statistic, in order to be conservative. We keep θ_{13} and θ_{12} fixed at their present-day best-fit values [82]. For θ_{13} , the precision that Daya Bay has achieved, of 2.8% [132], is not expected to be improved upon by upcoming experiments. For θ_{12} , whose present-day uncertainty is of 4.5%, we expect only weak sensitivity in the oscillation probabilities (see section 3.2), so fixing its value is a justified approximation. For the neutrino mass ordering, we adopt a simplified approach where switching from NMO to IMO amounts only to flipping the sign of Δm_{31}^2 to make it negative. This approach is motivated by the fact that the present-day 3σ allowed ranges of the mixing parameters are similar in the NMO and IMO [82, 92, 93], except for δ_{CP} and Δm_{31}^2 . (Further, in the next decade, DUNE is expected to determine the mass ordering, though, admittedly, non-standard oscillations like those induced by long-range interactions may confound this [56].)

Below, we compute the test-statistics by varying the long-range matter potential in the range $10^{-15} \leq V_{\alpha\beta}/\text{eV} \leq 3 \times 10^{-13}$, where its effects are potentially visible in DUNE and T2HK. This range is wide enough to comfortably place constraints or make measurements with significant statistical confidence.

4.2 Projected constraints on long-range interactions

Figure 5 shows how the test-statistics for constraints, e.g., eq. (4.7), vary with the potential, for the three symmetries and for DUNE, T2HK, and their combination. As expected, they are smallest closer to the true value of the potential, $V_{\alpha\beta}^{\text{true}} = 0$, and grow as they move away from it. At high values of $V_{\alpha\beta}$, the test-statistics for DUNE and T2HK dip, reflecting a loss of sensitivity due to $V_{\alpha\beta}$ being degenerate with θ_{23} and δ_{CP} . Appendix B expands on this. Combining DUNE and T2HK removes the dips: T2HK lifts the degeneracies due to θ_{23} and δ_{CP} , while DUNE fixes the mass ordering, i.e., the sign of Δm_{31}^2 . Thus, our results reveal novel insight: *the interplay of DUNE and T2HK facilitates degeneracy-free constraints on flavor-dependent long-range neutrino interactions.*

Table 3 shows the resulting upper limits on the potential. They are strongest for $V_{\mu\tau}$, followed by $V_{e\tau}$ and then $V_{e\mu}$. For DUNE, the limits are driven predominantly by the runs in neutrino mode, which contribute most of the total event rate; see table 2 and figure 4. For T2HK, the runs in neutrino and antineutrino modes contribute comparably. For $L_\mu - L_\tau$, the limits on $V_{\mu\tau}$ are strongest because long-range interactions affect mainly the disappearance probabilities, $\nu_\mu \rightarrow \nu_\mu$ and $\bar{\nu}_\mu \rightarrow \bar{\nu}_\mu$ (see figure 3), whose associated disappearance detection channels have high event rates (see figure 4), making deviations from standard oscillations easier to spot. For $L_e - L_\tau$, long-range interactions enhance instead the appearance probabilities, $\nu_\mu \rightarrow \nu_e$ and $\bar{\nu}_\mu \rightarrow \bar{\nu}_e$, but the appearance detection channels have lower rates, so the limits on $V_{e\tau}$ are weaker. For $L_e - L_\mu$, long-range interactions affect both the appearance probabilities — though less so than under the other two symmetries — and the disappearance probabilities — though less so than under the $L_\mu - L_\tau$ symmetry; as a result, the limits on $V_{e\mu}$ are the weakest. Figure 6 (also figure 1) shows the corresponding upper limits on $G'_{\alpha\beta}$ (refer to eq. (2.7)) for varying $m'_{\alpha\beta}$, translated from the upper limits on $V_{\alpha\beta}$ in table 3 via the definition of the potential, eq. (2.8). Each curve in figure 6 is an isocontour of potential that saturates each of the upper limits in table 3. The curves show step-like transitions at various values of $m'_{\alpha\beta}$: as explained

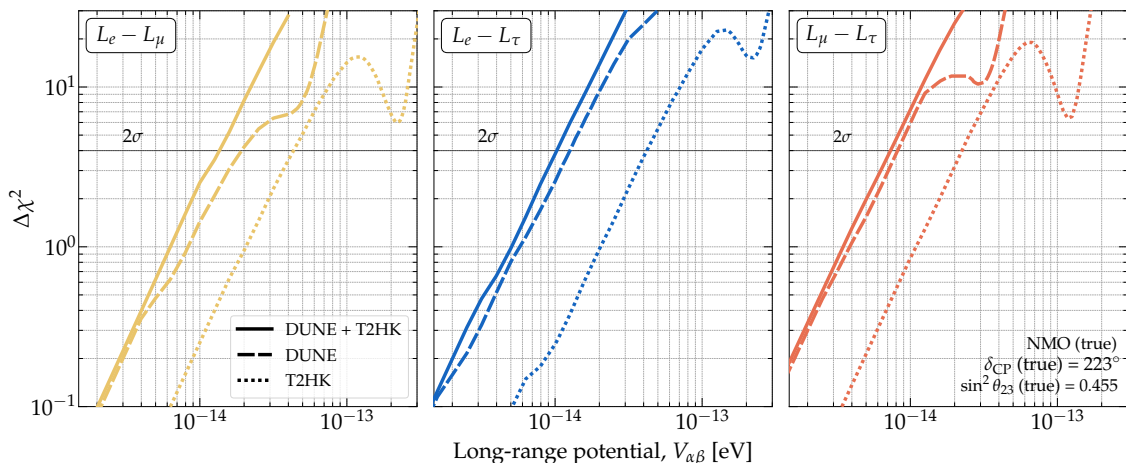


Figure 5. Projected test-statistic used to constrain the long-range matter potentials $V_{e\mu}$, $V_{e\tau}$, and $V_{\mu\tau}$, using DUNE, T2HK, and their combination. The $\Delta\chi^2$ function is eq. (4.7) and similar ones, assuming $V_{\alpha\beta}^{\text{true}} = 0$ for the true value of the potentials. We profile over the values of the most relevant standard mixing parameters and over the neutrino mass ordering; see table 1. See table 3 for the resulting upper limits on the potentials and figure 6 for the corresponding constraints on the mass and coupling of the new mediator. Combining DUNE and T2HK not only provides sensitivity to lower values of the potential, but also removes degeneracies in the test-statistics that would otherwise weaken the sensitivity. See sections 4.1 and 4.2 for details.

Detector	Upper limits (2σ) on potential [10^{-14} eV]		
	$V_{e\mu}$	$V_{e\tau}$	$V_{\mu\tau}$
DUNE	1.9	1.3	0.82
T2HK	4.4	4.2	2.2
DUNE + T2HK	1.4	1.0	0.73

Table 3. Projected upper limits (2σ) on the long-range matter potentials $V_{e\mu}$, $V_{e\tau}$, and $V_{\mu\tau}$, using DUNE, T2HK, and their combination. See figure 5 for the test-statistics from whence they originate and figure 6 for constraints on the mass and coupling of the associated mediator. See sections 4.1 and 4.2 for details.

in ref. [7] (see also section 2.2), each transition reflects the interaction range becoming long enough for a new source of electrons or neutrons to contribute to the total potential, eq. (2.8). For $m'_{\alpha\beta} \sim 10^{-18}$ – 10^{-10} eV, the Earth and the Moon dominate the upper limits; for $m'_{\alpha\beta} \lesssim 10^{-18}$ eV, the Sun dominates; for $m'_{\alpha\beta} \lesssim 10^{-27}$ eV, the Milky Way dominates; and, for $m'_{\alpha\beta} \lesssim 10^{-33}$ eV, cosmological electrons and neutrinos dominate.

Down to $m'_{\alpha\beta} \sim 10^{-18}$ eV, where direct limits on flavor-dependent long-range neutrino interactions exist, our projected limits improve on existing ones that use atmospheric neutrinos [2], are comparable to limits that use solar, reactor [3], and accelerator neutrinos [54], and to limits culled from non-standard interactions [4–6], but are weaker than limits from a global fit to oscillation data [1].

Below $m'_{\alpha\beta} \sim 10^{-18}$ eV, our projected limits tread into a largely unexplored range. To our knowledge, the only constraints that exist there, other than the indirect, tentative one

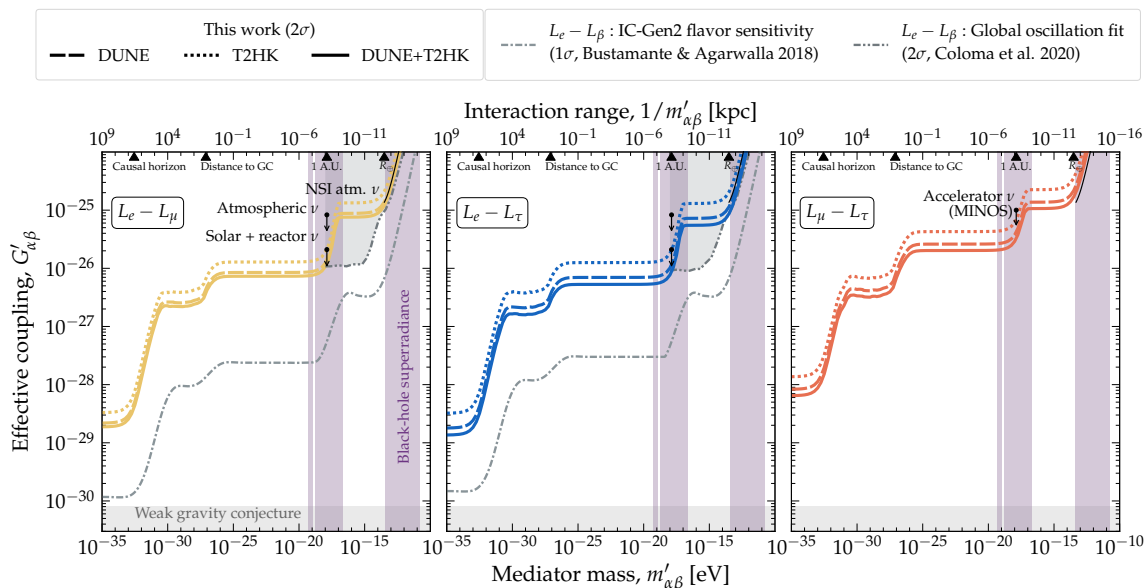


Figure 6. Projected upper limits on the effective coupling, $G'_{\alpha\beta}$ (eq. (2.7)), of the new boson, $Z'_{\alpha\beta}$, with mass $m'_{\alpha\beta}$, that mediates flavor-dependent long-range neutrino interactions, using DUNE, T2HK, and their combination. Same as figure 1, but now showing also limits using DUNE and T2HK separately. *Left:* for neutrino-electron interactions under the $L_e - L_\mu$ symmetry. *Center:* for neutrino-electron interactions under $L_e - L_\tau$. *Right:* for neutrino-neutron interactions under $L_\mu - L_\tau$; existing limits from accelerator neutrinos in MINOS (95% C.L.) are from ref. [54], and for non-standard interactions (NSI) we follow appendix C in ref. [80]. See section 4.2 for details.

from the weak gravity conjecture [10], are from measurements of the flavor composition of high-energy astrophysical neutrinos in the IceCube neutrino telescope, from ref. [7], which, however, were only produced at the 1σ level as a proof of principle of the sensitivity. A recent recalculation [80] found comparable results at higher statistical significance, using more solid statistical methods. Ideally, the sensitivity that could be reaped from high-energy astrophysical neutrinos is unmatched due to them having energies in the TeV–PeV range — which enhances the possible contribution of long-range interactions relative to standard oscillations — and to the fact that neutrinos of all flavors are detected. However, it is presently downplayed by large astrophysical uncertainties, limited event rates, and the difficulty in measuring the flavor composition in neutrino telescopes. These issues will likely be surmounted in the future [133–135]. For now, figure 6 shows the projected proof-of-principle sensitivity of the envisioned IceCube-Gen2 upgrade [95], from ref. [7]. Our limits from DUNE and T2HK improve on it significantly due to high event rates and well-characterized neutrino beams.

4.3 Discovering subdominant long-range interactions

Figure 7 shows the inferred allowed ranges of the coupling, for varying mediator mass, for three illustrative choices of the true value of the long-range potential, one for each symmetry: $V_{e\mu}^{\text{true}} = 2.12 \times 10^{-14}$ eV, $V_{e\tau}^{\text{true}} = 1.6 \times 10^{-14}$ eV, and $V_{\mu\tau}^{\text{true}} = 1.12 \times 10^{-14}$ eV.

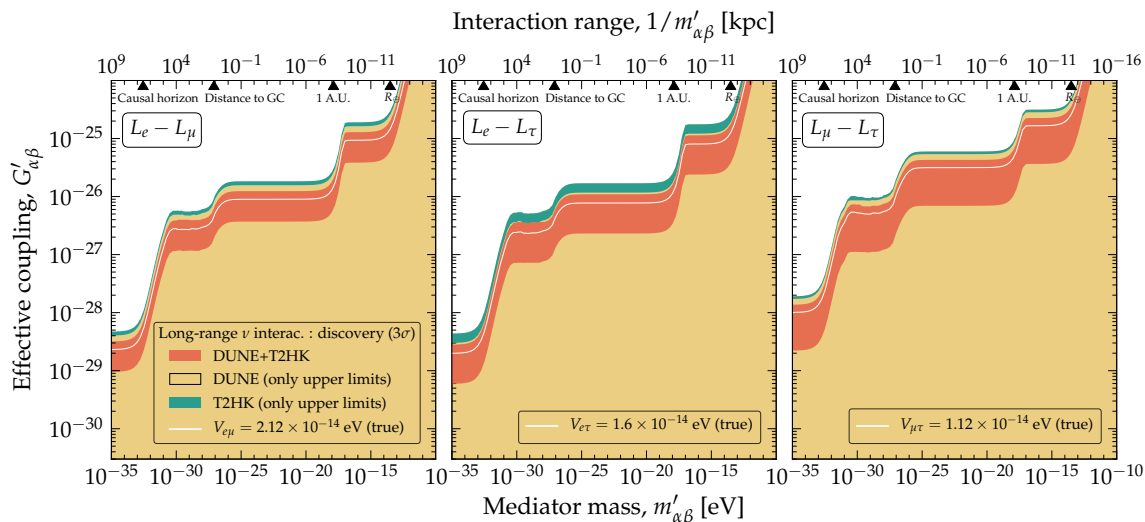


Figure 7. Projected discovery potential of flavor-dependent long-range neutrino interactions. We show allowed ranges (3σ) of the effective coupling, $G'_{\alpha\beta}$ (eq. (2.7)), of the new boson, $Z'_{\alpha\beta}$, with mass $m'_{\alpha\beta}$, that mediates the interactions, using DUNE, T2HK, and their combination. The $\Delta\chi^2$ function is eq. (4.7) and similar ones, fixing the true value of the long-range potential, $V_{\alpha\beta}^{\text{true}}$, at test values chosen to make the long-range interactions subdominant. Like in figure 6, we either fix or profile over the standard mixing parameters and the neutrino mass ordering; see table 1. See related figures 8 and 9. *DUNE or T2HK may not be able to discover long-range interactions separately, but their combination may.* See sections 4.1 and 4.3 for details.

They represent long-range interactions that are subdominant to standard oscillations; see section 2.3. To generate figure 7, first we compute the allowed ranges of $V_{\alpha\beta}$ using the discovery test-statistics, e.g., eq. (4.7) with $V_{\alpha\beta}^{\text{true}}$ fixed to the above illustrative choices, and then we use eq. (2.8) to translate those into allowed ranges of $G'_{\alpha\beta}$ for different values of $m'_{\alpha\beta}$. We present results for a modest discovery significance of 3σ .

Figure 7 shows that DUNE and T2HK, by themselves, can only place upper limits on $G'_{\alpha\beta}$. Thus, our discovery forecasts also reveal novel insight: *DUNE and T2HK, by themselves, may be unable to discover subdominant long-range interactions, but their combined action may.* For the illustrative choices of the potentials, the allowed 3σ ranges combining DUNE and T2HK are $V_{e\mu} \in [3.62 \times 10^{-15}, 4.04 \times 10^{-14}]$ eV, $V_{e\tau} \in [1.41 \times 10^{-15}, 3.13 \times 10^{-14}]$ eV, and $V_{\mu\tau} \in [5.87 \times 10^{-16}, 2.24 \times 10^{-14}]$ eV, implying a relative measurement uncertainty of 90%–100%. For larger values of the true potential, discovery claims should be stronger and the uncertainty in its measurement should shrink.

Figures 8 and 9 reveal that the reason behind the difficulty of T2HK and DUNE to discover subdominant long-range interactions by themselves are the uncertainties in δ_{CP} , θ_{23} , and the neutrino mass ordering. Appendix B shows this in detail; here we summarize. On the one hand, in T2HK, the shorter baseline provides less contamination from fake CP violation induced by SM matter effects and, therefore, higher precision in measuring δ_{CP} [136–140], while the high event rates in the disappearance channels provide high precision on θ_{23} . However, at the same time, the shorter baseline reduces the sensitivity to the

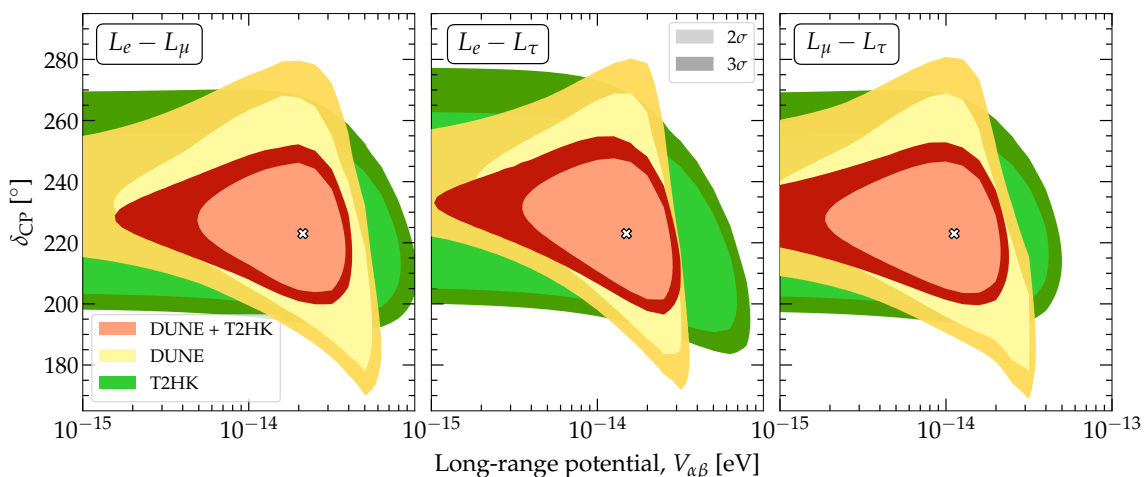


Figure 8. Allowed regions of the long-range potential, $V_{\alpha\beta}$, and the CP-violating phase, δ_{CP} . The true values of the potentials are the same as in figure 7. The test-statistic is profiled over $\sin^2 \theta_{23}$, $|\Delta m_{31}^2|$, and the mass ordering; see, e.g., eq. (4.8). See sections 4.1 and 4.3 for details.

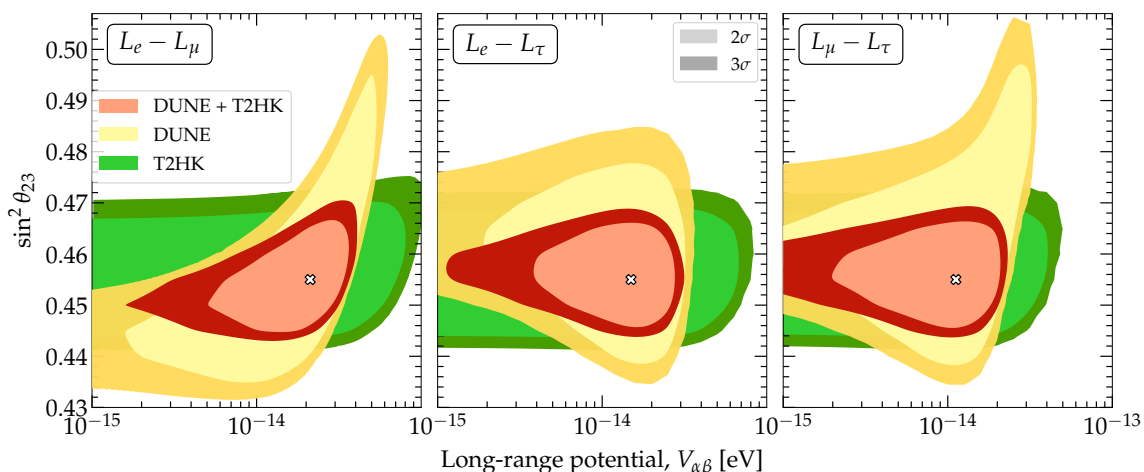


Figure 9. Allowed regions of the long-range potential, $V_{\alpha\beta}$, and the atmospheric mixing angle, $\sin^2 \theta_{23}$. Same as figure 8, but profiling the test-statistic instead over δ_{CP} , $|\Delta m_{31}^2|$, and the mass ordering; see, e.g., eq. (4.9). See sections 4.1 and 4.3 for details.

mass ordering and provides a shorter neutrino travel time during which long-range interactions may act. On the other hand, in DUNE, the longer baseline helps to pin down the mass ordering, but introduces more contamination from fake CP violation, which degrades the sensitivity to δ_{CP} compared to T2HK. Also, in the presence of long-range interactions, DUNE can measure θ_{23} significantly less precisely than T2HK.

Thus, combining DUNE and T2HK improves the sensitivity with which δ_{CP} , θ_{23} , and the mass ordering can be measured, weakens the degeneracies between them and the long-range potential, and allows for its measurement at a high statistical significance.

5 Summary and outlook

Neutrinos are powerful probes of new physics. Extant uncertainties in their properties leave room for the conceivable possibility that they experience interactions with matter beyond weak ones. Discovering them would not only further our view of neutrino physics, but also represent striking evidence of physics beyond the Standard Model. In the 2030s, the next-generation long-baseline neutrino experiments DUNE and T2HK may provide us with an opportunity to look for new neutrino interactions more incisively than ever before, thanks to high event rates and well-characterized neutrino beams. We have forecast their reach. Because we use detailed simulations of the detectors, including efficiencies, run times, and backgrounds, our predictions are realistic.

Our forecasts are geared at new flavor-dependent neutrino interactions that are introduced by gauging three different accidental global lepton-number symmetries of the Standard Model, generated by $L_e - L_\mu$, $L_e - L_\tau$, and $L_\mu - L_\tau$, that have received prior attention in other experimental settings [1–3, 7, 8, 54, 56, 58]. We focus on them because they can be gauged anomaly-free, so the only new particle introduced is a neutral vector boson that mediates the interaction. Its mass and coupling strength are a priori undetermined. Gauging $L_e - L_\mu$ and $L_e - L_\tau$ introduces new neutrino-electron interactions. Gauging $L_\mu - L_\tau$ introduces new neutrino-neutron interactions.

Under these interactions, electrons and neutrons source a flavor-dependent potential that may affect neutrino oscillations. We concentrate on ultra-light mediators, with masses below 10^{-10} eV. They induce interactions whose range is ultra-long — ranging from hundreds of meters to Gpc, depending on the mass — so that neutrinos may experience the potential sourced by a large number of nearby and distant electrons and neutrons in the Earth, the Moon, the Sun, the Milky Way, and the cosmological matter distribution [7]. Yet, because the coupling strength may be tiny, their effects on the oscillation probabilities may be subtle and, therefore, testable with future experiments, like DUNE and T2HK.

Our forecasts reveal two novel, promising perspectives. First, while DUNE and T2HK, individually, should be able to improve on present-day upper limits on the coupling strength of the new interaction, their individual sensitivities are hampered by degeneracies due to uncertainties in the mixing angle θ_{23} , the CP-violating phase, δ_{CP} , and the neutrino mass ordering. Yet, DUNE and T2HK have complementary capabilities: while T2HK is especially well-suited to measure θ_{23} and δ_{CP} , DUNE is especially well-suited to measure the neutrino mass ordering. Thus, *combining DUNE and T2HK removes parameter degeneracies, which tightens the upper limits on long-range neutrino interactions.* Second, and more importantly, *neither DUNE nor T2HK, by itself, may discover subdominant long-range interactions, owing to parameter degeneracies, but their combination may.* Thus, our forecasts stress the need for combining measurements in DUNE and T2HK to probe long-range interactions.

More broadly, our results illustrate the known need for complementarity in the future long-baseline neutrino program, not only to measure the standard mixing parameters, but to search for new physics. For flavor-dependent long-range neutrino interactions, a future global fit to oscillation data is poised to deliver substantially improved limits or transformative discovery.

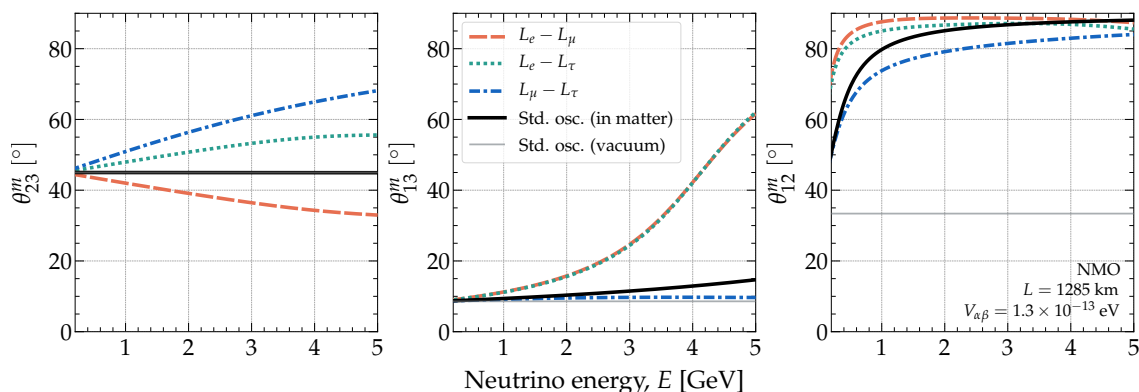


Figure 10. Variation of the effective neutrino mixing angles with neutrino energy, for the three lepton-number symmetries, $L_\alpha - L_\beta$. For this plot, we adopt the baseline, average matter potential, and approximate energy range of DUNE; see section 3.1.1. For all the symmetries, we adopt an illustrative value of the new matter potential of $V_{\alpha\beta} = 1.3 \times 10^{-13}$ eV. For comparison, we include results using only standard matter effects and in a vacuum. The values of the mixing parameters in vacuum are from table 1, except with $\sin^2 \theta_{23} = 0.5$. See appendix A for details.

Acknowledgments

We thank Pilar Coloma, Sudipta Das, Iván Esteban, Shirley Li, Swapna Mahapatra, Ashish Narang, and Yu-Dai Tsai for their helpful discussions and crucial input. S.K.A. acknowledges the support from the Department of Atomic Energy (DAE), Govt. of India, under the Project Identification no. RIO 4001. S.K.A. acknowledges the financial support from the Swarnajayanti Fellowship (sanction order no. DST/SJF/PSA-05/2019-20) provided by the Department of Science and Technology (DST), Govt. of India, and the Research Grant (sanction order no. SB/SJF/2020-21/21) provided by the Science and Engineering Research Board (SERB), Govt. of India, under the Swarnajayanti Fellowship project. S.K.A. would like to thank the United States-India Educational Foundation (USIEF) for providing the financial support through the Fulbright-Nehru Academic and Professional Excellence Fellowship (Award no. 2710/F-N APE/2021). M.S. acknowledges the financial support from the DST, Govt. of India (DST/INSPIRE Fellowship/2018/IF180059). M.B. is supported by the VILLUM FONDEN under the project no. 29388. The numerical simulations are carried out using the “SAMKHYA: High-Performance Computing Facility” at the Institute of Physics, Bhubaneswar, India.

A Effects of long-range interactions on neutrino oscillation parameters

Figures 10 and 11 show the variation with neutrino energy of, respectively, the mixing angles and mass splittings under the new matter interactions for the three symmetries, and geared at DUNE for illustration. Their behavior when geared at T2HK is similar.

Regarding the mixing angles, their behavior in figure 10 backs the explanation of the behavior of the oscillation probabilities in section 3.2, in agreement with refs. [56, 58, 90].

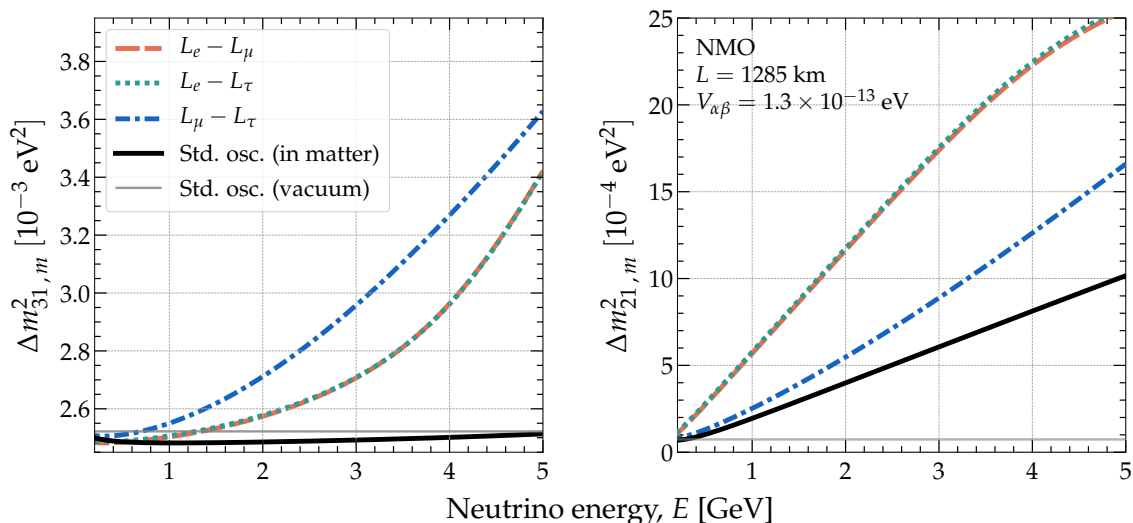


Figure 11. Variation of the effective neutrino mass splittings with neutrino energy, for the three lepton-number symmetries, $L_\alpha - L_\beta$. Same as figure 10, but for the mass splittings. See appendix A for details.

Regarding the mass splittings, the energy at which the first oscillation maximum occurs in the probabilities (figure 3) is determined mostly by $\Delta m_{31,m}^2$. Figure 11 shows that, under $L_e - L_\mu$ and $L_e - L_\tau$, $\Delta m_{31,m}^2$ evolves similarly with energy; this explains why the oscillation maxima for these two symmetries occur at approximately the same energy. The change with energy of $\Delta m_{21,m}^2$ affects the $\nu_\mu \rightarrow \nu_\mu$ and $\nu_\mu \rightarrow \nu_\tau$ probabilities, but only for baselines of around 10000 km, as shown in ref. [89].

B Effects of oscillation parameter uncertainties on constraints

Table 4 illustrates how the uncertainty on different oscillation parameters affect the constraint the test-statistic, $\Delta\chi^2$, i.e., eq. (4.7) and similar ones, via profiling over them. The table reports the test-statistic computed assuming that the true value of the potential is $V_{\alpha\beta}^{\text{true}} = 0$, and evaluated at an illustrative test value of $V_{\alpha\beta} = 3 \times 10^{-14}$ eV. The observations we make regarding table 4 hold also for other test values of $V_{\alpha\beta}$. Our main results are computed by profiling the test-statistic over δ_{CP} , $\sin^2 \theta_{23}$, $|\Delta m_{31}^2|$, and o . Table 4 shows what the effect is of profiling only over one or two of them at a time.

Because DUNE can measure $|\Delta m_{31}^2|$ and the mass ordering precisely, profiling over their values has little effect compared to keeping them fixed. Similarly, because T2HK can measure θ_{23} and δ_{CP} precisely, profiling over their values has little effect compared to keeping them fixed. Combining DUNE and T2HK affords both.

Profiling over $\sin^2 \theta_{23}$ and δ_{CP} has the largest effect on the test-statistic. The shrinking of $\Delta\chi^2$ by profiling over $\sin^2 \theta_{23}$, compared to keeping it fixed, comes via the $\nu_\mu \rightarrow \nu_\mu$ and $\bar{\nu}_\mu \rightarrow \bar{\nu}_\mu$ disappearance probabilities, which are $\propto \sin^2 \theta_{23}$ (see, e.g., eq. (33) in ref. [87]). The shrinking of $\Delta\chi^2$ by profiling over δ_{CP} comes instead via the $\nu_\mu \rightarrow \nu_e$ and $\bar{\nu}_\mu \rightarrow \bar{\nu}_e$ appearance probabilities, which depend on δ_{CP} . Thus, under $L_e - L_\mu$, the test-statistic is

Parameters in test event spectra	Test-statistic, $\Delta\chi^2$								
	$L_e - L_\mu$			$L_e - L_\tau$			$L_\mu - L_\tau$		
	D	T	D+T	D	T	D+T	D	T	D+T
Fixed δ_{CP} , $\sin^2 \theta_{23}$, $ \Delta m_{31}^2 $, o	23	8	25	37	10	41	50	18	58
Profiled over δ_{CP} only	22	7	25	20	3	31	44	16	54
Profiled over $\sin^2 \theta_{23}$ only	10	2	19	35	8	40	25	8	48
Profiled over $ \Delta m_{31}^2 $ and o only	23	5	25	37	7	41	50	15	58
Profiled over δ_{CP}, $\sin^2 \theta_{23}$, Δm_{31}^2, o	6	2	19	18	3	31	11	7	44

Table 4. Effect of profiling over the different parameters on the test-statistic for constraints. The test-statistic is computed using eq. (4.7), assuming $V_{\alpha\beta}^{\text{true}} = 0$. In this table, we report the values of the test-statistic calculated at an illustrative choice of the potential, $V_{\alpha\beta} = 3 \times 10^{-14}$ eV. We show effects separately for DUNE (D), T2HK (T), and their combination (D+T). Our main results are obtained by profiling over δ_{CP} , $\sin^2 \theta_{23}$, $|\Delta m_{31}^2|$, and the neutrino mass ordering, o , i.e., the sign of Δm_{31}^2 , in our prescription (see section 4.1). Results for partial profiling are shown only for the purpose of singling out the effect of different parameters. The values of the parameters that are not profiled over are fixed to the benchmark values in table 1.

	Standard mixing parameters (IMO)					
	$\sin^2 \theta_{12}$	$\sin^2 \theta_{23}$	$\sin^2 \theta_{13}$	$\frac{\Delta m_{31}^2}{10^{-3} \text{ eV}^2}$	$\frac{\Delta m_{21}^2}{10^{-5} \text{ eV}^2}$	$\delta_{\text{CP}} (\circ)$
Benchmark	0.303	0.569	0.0223	2.418	7.36	274
Status in fits	Fixed	Minimized	Fixed	Minimized	Fixed	Minimized
Range	–	[0.4, 0.6]	–	[2.341, 2.501]	–	[193, 342]

Table 5. Values of the standard mixing parameters used in our analysis, assuming that the true neutrino mass ordering is inverted. Same as table 1, made assuming that the true mass ordering is normal, but instead assuming that it is inverted (IMO). The benchmark values are the best-fit values from ref. [82].

driven by the uncertainty in $\sin^2 \theta_{23}$ and δ_{CP} — via profiling over them; under $L_e - L_\tau$, it is driven mostly by δ_{CP} ; and, under $L_\mu - L_\tau$, it is driven mostly by $\sin^2 \theta_{23}$.

C Constraints assuming inverted mass ordering

In the main text, we showed results obtained assuming that the true neutrino mass ordering is normal. Here we show constraints assuming instead that the true ordering is inverted. They are broadly similar to the ones obtained under normal ordering (section 4.2).

Table 5 shows the values and allowed ranges of the mixing parameters that we use when assuming that the inverted mass ordering is true, taken from the global oscillation fit of ref. [82]. The values are similar as for normal ordering (table 3), with the important difference that for inverted ordering the benchmark value of θ_{23} lies in the higher octant, which has consequences for the sensitivity, as we point out below.

Figure 5 shows how the test-statistics for constraints, e.g., eq. (4.7), vary with the long-range potential, for the three symmetries and for DUNE, T2HK, and their combination,

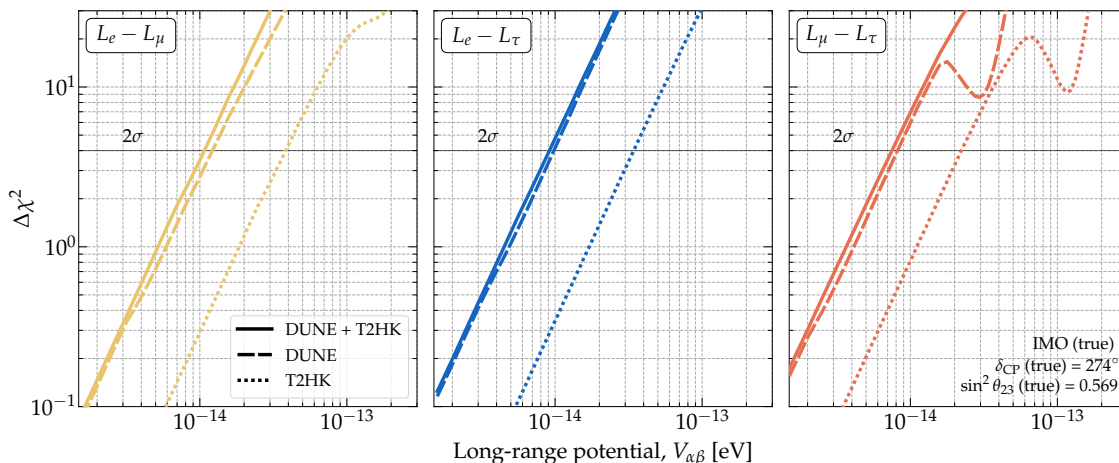


Figure 12. Projected test-statistic used to constrain the long-range matter potentials $V_{e\mu}$, $V_{e\tau}$, and $V_{\mu\tau}$, using DUNE, T2HK, and their combination, assuming that the true neutrino mass ordering is inverted. Same as figure 5, made assuming that the true mass ordering is normal, but instead assuming that it is inverted. See table 6 for the resulting upper limits on the potentials. See sections 4.1 and 4.2 in the main text, and appendix C for details.

Detector	Upper limit (2σ) on potential [10^{-14} eV]		
	$V_{e\mu}$	$V_{e\tau}$	$V_{\mu\tau}$
DUNE	0.99	3.4	0.92
T2HK	1.2	3.9	1.1
DUNE + T2HK	0.82	2.2	0.75

Table 6. Projected upper limits (2σ) on the long-range matter potentials $V_{e\mu}$, $V_{e\tau}$, and $V_{\mu\tau}$, using DUNE, T2HK, and their combination, assuming that the true neutrino mass ordering is inverted. Same as table 3, made assuming that the true mass ordering is normal, but instead assuming that it is inverted. See figure 12 for the test-statistics from whence they originate and figure 6. See sections 4.1 and 4.2, and appendix C for details.

assuming the true mass ordering is inverted. Their behavior is broadly similar to that in figure 6 for normal ordering. However, in figure 12 the weakening of the sensitivity due to parameter degeneracies is milder than in figure 5 because, assuming inverted mass ordering, θ_{23} lies in the higher octant, which lessens the influence of δ_{CP} [136, 140].

Table 6 shows the resulting upper limits on the long-range potentials. Like for normal ordering (table 3), they are strongest for $V_{\mu\tau}$. Compared to normal ordering, the limits on $V_{e\mu}$ are stronger by a factor of 2 or more, and the limits on $V_{e\tau}$ are similarly weaker.

D Normalization errors in event rates

Table 7 shows the systematic normalization errors on the signal, $\pi_{e,c}^s$ and background event rates, $\pi_{e,c,k}^b$, of DUNE [17] and T2HK [18]. In section 4.1, we use them to compute test event spectra, eq. (4.3), as part of computing the test-statistic.

Experiment	Normalization errors [%]							
	Signal, $\pi_{e,c}^s$				Background, $\pi_{e,c,k}^b$			
	App. ν	App. $\bar{\nu}$	Disapp. ν	Disapp. $\bar{\nu}$	$\nu_e, \bar{\nu}_e$ CC	$\nu_\mu, \bar{\nu}_\mu$ CC	$\nu_\tau, \bar{\nu}_\tau$ CC	NC
DUNE	2	2	5	5	5	5	20	10
T2HK	5	5	3.5	3.5	10	10	–	10

Table 7. Normalization errors of the event rates associated to the signal and background detection channels in DUNE and T2HK. They are shown separately for the neutrino (ν) and antineutrino ($\bar{\nu}$) modes, and for the appearance (“App.”) and disappearance (“Disapp.”) channels. Normalization errors are used to compute test event spectra, eq. (4.3). The values are taken from refs. [17, 18]. See section 4.1 for details.

Open Access. This article is distributed under the terms of the Creative Commons Attribution License (CC-BY 4.0), which permits any use, distribution and reproduction in any medium, provided the original author(s) and source are credited.

References

- [1] P. Coloma, M.C. Gonzalez-Garcia and M. Maltoni, *Neutrino oscillation constraints on $U(1)$ ’ models: from non-standard interactions to long-range forces*, *JHEP* **01** (2021) 114 [Erratum *ibid.* **11** (2022) 115] [[arXiv:2009.14220](#)] [[INSPIRE](#)].
- [2] A.S. Joshipura and S. Mohanty, *Constraints on flavor dependent long range forces from atmospheric neutrino observations at super-Kamiokande*, *Phys. Lett. B* **584** (2004) 103 [[hep-ph/0310210](#)] [[INSPIRE](#)].
- [3] A. Bandyopadhyay, A. Dighe and A.S. Joshipura, *Constraints on flavor-dependent long range forces from solar neutrinos and KamLAND*, *Phys. Rev. D* **75** (2007) 093005 [[hep-ph/0610263](#)] [[INSPIRE](#)].
- [4] SUPER-KAMIOKANDE collaboration, *Study of Non-Standard Neutrino Interactions with Atmospheric Neutrino Data in Super-Kamiokande I and II*, *Phys. Rev. D* **84** (2011) 113008 [[arXiv:1109.1889](#)] [[INSPIRE](#)].
- [5] T. Ohlsson, *Status of non-standard neutrino interactions*, *Rept. Prog. Phys.* **76** (2013) 044201 [[arXiv:1209.2710](#)] [[INSPIRE](#)].
- [6] M.C. Gonzalez-Garcia and M. Maltoni, *Determination of matter potential from global analysis of neutrino oscillation data*, *JHEP* **09** (2013) 152 [[arXiv:1307.3092](#)] [[INSPIRE](#)].
- [7] M. Bustamante and S.K. Agarwalla, *Universe’s Worth of Electrons to Probe Long-Range Interactions of High-Energy Astrophysical Neutrinos*, *Phys. Rev. Lett.* **122** (2019) 061103 [[arXiv:1808.02042](#)] [[INSPIRE](#)].
- [8] M.B. Wise and Y. Zhang, *Lepton Flavorful Fifth Force and Depth-dependent Neutrino Matter Interactions*, *JHEP* **06** (2018) 053 [[arXiv:1803.00591](#)] [[INSPIRE](#)].
- [9] M. Baryakhtar, R. Lasenby and M. Teo, *Black Hole Superradiance Signatures of Ultralight Vectors*, *Phys. Rev. D* **96** (2017) 035019 [[arXiv:1704.05081](#)] [[INSPIRE](#)].
- [10] N. Arkani-Hamed, L. Motl, A. Nicolis and C. Vafa, *The String landscape, black holes and gravity as the weakest force*, *JHEP* **06** (2007) 060 [[hep-th/0601001](#)] [[INSPIRE](#)].
- [11] T.D. Lee and C.-N. Yang, *Conservation of Heavy Particles and Generalized Gauge Transformations*, *Phys. Rev.* **98** (1955) 1501 [[INSPIRE](#)].

- [12] L. Okun, *Leptons and photons*, *Phys. Lett. B* **382** (1996) 389 [[hep-ph/9512436](#)] [[INSPIRE](#)].
- [13] J.G. Williams, X.X. Newhall and J.O. Dickey, *Relativity parameters determined from lunar laser ranging*, *Phys. Rev. D* **53** (1996) 6730 [[INSPIRE](#)].
- [14] A.D. Dolgov, *Long range forces in the universe*, *Phys. Rept.* **320** (1999) 1 [[INSPIRE](#)].
- [15] E.G. Adelberger, B.R. Heckel and A.E. Nelson, *Tests of the gravitational inverse square law*, *Ann. Rev. Nucl. Part. Sci.* **53** (2003) 77 [[hep-ph/0307284](#)] [[INSPIRE](#)].
- [16] J.G. Williams, S.G. Turyshev and D.H. Boggs, *Progress in lunar laser ranging tests of relativistic gravity*, *Phys. Rev. Lett.* **93** (2004) 261101 [[gr-qc/0411113](#)] [[INSPIRE](#)].
- [17] DUNE collaboration, *Experiment Simulation Configurations Approximating DUNE TDR*, [arXiv:2103.04797](#) [[INSPIRE](#)].
- [18] HYPER-KAMIOKANDE collaboration, *Physics potentials with the second Hyper-Kamiokande detector in Korea*, *PTEP* **2018** (2018) 063C01 [[arXiv:1611.06118](#)] [[INSPIRE](#)].
- [19] HYPER-KAMIOKANDE collaboration, *Hyper-Kamiokande Design Report*, [arXiv:1805.04163](#) [[INSPIRE](#)].
- [20] C.A. Argüelles et al., *New opportunities at the next-generation neutrino experiments I: BSM neutrino physics and dark matter*, *Rept. Prog. Phys.* **83** (2020) 124201 [[arXiv:1907.08311](#)] [[INSPIRE](#)].
- [21] C.A. Argüelles et al., *Snowmass white paper: beyond the standard model effects on neutrino flavor: Submitted to the proceedings of the US community study on the future of particle physics (Snowmass 2021)*, *Eur. Phys. J. C* **83** (2023) 15 [[arXiv:2203.10811](#)] [[INSPIRE](#)].
- [22] J.M. Berryman et al., *Neutrino self-interactions: A white paper*, *Phys. Dark Univ.* **42** (2023) 101267 [[arXiv:2203.01955](#)] [[INSPIRE](#)].
- [23] P. Coloma, L.W. Koerner, I.M. Shoemaker and J. Yu, *Neutrino Frontier Topical Group Report (NF03): Physics Beyond the Standard Model*, [arXiv:2209.10362](#) [[INSPIRE](#)].
- [24] P. Huber et al., *Snowmass Neutrino Frontier Report*, in the proceedings of the *Snowmass 2021*, (2022) [[arXiv:2211.08641](#)] [[INSPIRE](#)].
- [25] W. Altmannshofer et al., *Neutrino Tridents at DUNE*, *Phys. Rev. D* **100** (2019) 115029 [[arXiv:1902.06765](#)] [[INSPIRE](#)].
- [26] P. Ballett et al., *Z's in neutrino scattering at DUNE*, *Phys. Rev. D* **100** (2019) 055012 [[arXiv:1902.08579](#)] [[INSPIRE](#)].
- [27] V. De Romeri, K.J. Kelly and P.A.N. Machado, *DUNE-PRISM Sensitivity to Light Dark Matter*, *Phys. Rev. D* **100** (2019) 095010 [[arXiv:1903.10505](#)] [[INSPIRE](#)].
- [28] DUNE collaboration, *Prospects for beyond the Standard Model physics searches at the Deep Underground Neutrino Experiment*, *Eur. Phys. J. C* **81** (2021) 322 [[arXiv:2008.12769](#)] [[INSPIRE](#)].
- [29] T. Schwetz, A. Zhou and J.-Y. Zhu, *Constraining active-sterile neutrino transition magnetic moments at DUNE near and far detectors*, *JHEP* **21** (2020) 200 [[arXiv:2105.09699](#)] [[INSPIRE](#)].
- [30] V. Mathur, I.M. Shoemaker and Z. Tabrizi, *Using DUNE to shed light on the electromagnetic properties of neutrinos*, *JHEP* **10** (2022) 041 [[arXiv:2111.14884](#)] [[INSPIRE](#)].

- [31] F. Capozzi et al., *Extending the reach of leptophilic boson searches at DUNE and MiniBooNE with bremsstrahlung and resonant production*, *Phys. Rev. D* **104** (2021) 115010 [[arXiv:2108.03262](#)] [[INSPIRE](#)].
- [32] P.S.B. Dev et al., *Light, long-lived $B - L$ gauge and Higgs bosons at the DUNE near detector*, *JHEP* **07** (2021) 166 [[arXiv:2104.07681](#)] [[INSPIRE](#)].
- [33] K. Chakraborty, A. Das, S. Goswami and S. Roy, *Constraining general $U(1)$ interactions from neutrino-electron scattering measurements at DUNE near detector*, *JHEP* **04** (2022) 008 [[arXiv:2111.08767](#)] [[INSPIRE](#)].
- [34] M. Ovchinnikov, T. Schwetz and J.-Y. Zhu, *Dipole portal and neutrinophilic scalars at DUNE revisited: The importance of the high-energy neutrino tail*, *Phys. Rev. D* **107** (2023) 055029 [[arXiv:2210.13141](#)] [[INSPIRE](#)].
- [35] G. Chauhan, P.S.B. Dev and X.-J. Xu, *Probing the ν_R -philic Z' at DUNE near detectors*, *Phys. Lett. B* **841** (2023) 137907 [[arXiv:2204.11876](#)] [[INSPIRE](#)].
- [36] P.B. Denton, A. Giarnetti and D. Meloni, *How to identify different new neutrino oscillation physics scenarios at DUNE*, *JHEP* **02** (2023) 210 [[arXiv:2210.00109](#)] [[INSPIRE](#)].
- [37] S.K. Agarwalla, S. Das, S. Sahoo and P. Swain, *Constraining Lorentz invariance violation with next-generation long-baseline experiments*, *JHEP* **07** (2023) 216 [[arXiv:2302.12005](#)] [[INSPIRE](#)].
- [38] Y. Farzan and J. Heeck, *Neutrinophilic nonstandard interactions*, *Phys. Rev. D* **94** (2016) 053010 [[arXiv:1607.07616](#)] [[INSPIRE](#)].
- [39] S.K. Agarwalla, M. Ghosh and S.K. Raut, *A hybrid setup for fundamental unknowns in neutrino oscillations using T2HK (ν) and μ -DAR ($\bar{\nu}$)*, *JHEP* **05** (2017) 115 [[arXiv:1704.06116](#)] [[INSPIRE](#)].
- [40] J. Tang, Y. Zhang and Y.-F. Li, *Probing Direct and Indirect Unitarity Violation in Future Accelerator Neutrino Facilities*, *Phys. Lett. B* **774** (2017) 217 [[arXiv:1708.04909](#)] [[INSPIRE](#)].
- [41] P. Pasquini, *Long-Baseline Oscillation Experiments as a Tool to Probe High Energy Flavor Symmetry Models*, *Adv. High Energy Phys.* **2018** (2018) 1825874 [[arXiv:1802.00821](#)] [[INSPIRE](#)].
- [42] G.-J. Ding, Y.-F. Li, J. Tang and T.-C. Wang, *Confronting tridirect CP -symmetry models with neutrino oscillation experiments*, *Phys. Rev. D* **100** (2019) 055022 [[arXiv:1905.12939](#)] [[INSPIRE](#)].
- [43] A. Pal and Q. Shafi, *Supersymmetric $SU(5) \times U(1)_X$ and the weak gravity conjecture*, *Phys. Rev. D* **100** (2019) 043526 [[arXiv:1903.05703](#)] [[INSPIRE](#)].
- [44] K. Chakraborty, D. Dutta, S. Goswami and D. Pramanik, *Addendum to: Invisible neutrino decay: first vs second oscillation maximum*, *JHEP* **08** (2021) 136 [[arXiv:2012.04958](#)] [[INSPIRE](#)].
- [45] HYPER-KAMIOKANDE collaboration, *Hyper-Kamiokande Experiment: A Snowmass White Paper*, in the proceedings of the 2021 Snowmass Summer Study, (2022) [[arXiv:2203.02029](#)] [[INSPIRE](#)].
- [46] X.G. He, G.C. Joshi, H. Lew and R.R. Volkas, *New Z' phenomenology*, *Phys. Rev. D* **43** (1991) 22 [[INSPIRE](#)].

- [47] R. Foot, G.C. Joshi, H. Lew and R.R. Volkas, *Charge quantization in the standard model and some of its extensions*, *Mod. Phys. Lett. A* **5** (1990) 2721 [INSPIRE].
- [48] R. Foot, *New Physics From Electric Charge Quantization?*, *Mod. Phys. Lett. A* **6** (1991) 527 [INSPIRE].
- [49] X.-G. He, G.C. Joshi, H. Lew and R.R. Volkas, *Simplest Z' model*, *Phys. Rev. D* **44** (1991) 2118 [INSPIRE].
- [50] R. Foot, X.G. He, H. Lew and R.R. Volkas, *Model for a light Z' boson*, *Phys. Rev. D* **50** (1994) 4571 [hep-ph/9401250] [INSPIRE].
- [51] J.A. Grifols and E. Masso, *Neutrino oscillations in the sun probe long range leptonic forces*, *Phys. Lett. B* **579** (2004) 123 [hep-ph/0311141] [INSPIRE].
- [52] M. Honda et al., *Constraints on New Physics from Long Baseline Neutrino Oscillation Experiments*, [arXiv:0707.4545](https://arxiv.org/abs/0707.4545) [INSPIRE].
- [53] P. Langacker, *The Physics of Heavy Z' Gauge Bosons*, *Rev. Mod. Phys.* **81** (2009) 1199 [arXiv:0801.1345] [INSPIRE].
- [54] J. Heeck and W. Rodejohann, *Gauged $L_\mu - L_\tau$ and different Muon Neutrino and Anti-Neutrino Oscillations: MINOS and beyond*, *J. Phys. G* **38** (2011) 085005 [arXiv:1007.2655] [INSPIRE].
- [55] H. Davoudiasl, H.-S. Lee and W.J. Marciano, *Long-Range Lepton Flavor Interactions and Neutrino Oscillations*, *Phys. Rev. D* **84** (2011) 013009 [arXiv:1102.5352] [INSPIRE].
- [56] S.S. Chatterjee, A. Dasgupta and S.K. Agarwalla, *Exploring Flavor-Dependent Long-Range Forces in Long-Baseline Neutrino Oscillation Experiments*, *JHEP* **12** (2015) 167 [arXiv:1509.03517] [INSPIRE].
- [57] J. Heeck, M. Lindner, W. Rodejohann and S. Vogl, *Non-Standard Neutrino Interactions and Neutral Gauge Bosons*, *SciPost Phys.* **6** (2019) 038 [arXiv:1812.04067] [INSPIRE].
- [58] A. Khatun, T. Thakore and S. Kumar Agarwalla, *Can INO be Sensitive to Flavor-Dependent Long-Range Forces?*, *JHEP* **04** (2018) 023 [arXiv:1801.00949] [INSPIRE].
- [59] A.Y. Smirnov and X.-J. Xu, *Wolfenstein potentials for neutrinos induced by ultra-light mediators*, *JHEP* **12** (2019) 046 [arXiv:1909.07505] [INSPIRE].
- [60] A.S. Joshipura, N. Mahajan and K.M. Patel, *Generalised μ - τ symmetries and calculable gauge kinetic and mass mixing in $U(1)_{L_\mu - L_\tau}$ models*, *JHEP* **03** (2020) 001 [arXiv:1909.02331] [INSPIRE].
- [61] T. Kumar Poddar, S. Mohanty and S. Jana, *Vector gauge boson radiation from compact binary systems in a gauged $L_\mu - L_\tau$ scenario*, *Phys. Rev. D* **100** (2019) 123023 [arXiv:1908.09732] [INSPIRE].
- [62] T. Kumar Poddar, S. Mohanty and S. Jana, *Constraints on long range force from perihelion precession of planets in a gauged $L_e - L_{\mu,\tau}$ scenario*, *Eur. Phys. J. C* **81** (2021) 286 [arXiv:2002.02935] [INSPIRE].
- [63] J.A. Dror, *Discovering leptonic forces using nonconserved currents*, *Phys. Rev. D* **101** (2020) 095013 [arXiv:2004.04750] [INSPIRE].
- [64] P. Melas, D.K. Papoulias and N. Saoulidou, *Probing generalized neutrino interactions with the DUNE Near Detector*, *JHEP* **07** (2023) 190 [arXiv:2303.07094] [INSPIRE].

- [65] G. Alonso-Álvarez, K. Bleau and J.M. Cline, *Distortion of neutrino oscillations by dark photon dark matter*, *Phys. Rev. D* **107** (2023) 055045 [[arXiv:2301.04152](#)] [[INSPIRE](#)].
- [66] B. Pontecorvo, *Inverse beta processes and nonconservation of lepton charge*, *Zh. Eksp. Teor. Fiz.* **34** (1957) 247 [[INSPIRE](#)].
- [67] B. Pontecorvo, *Neutrino Experiments and the Problem of Conservation of Leptonic Charge*, *Zh. Eksp. Teor. Fiz.* **53** (1967) 1717 [[INSPIRE](#)].
- [68] V.N. Gribov and B. Pontecorvo, *Neutrino astronomy and lepton charge*, *Phys. Lett. B* **28** (1969) 493 [[INSPIRE](#)].
- [69] J. Hisano and D. Nomura, *Solar and atmospheric neutrino oscillations and lepton flavor violation in supersymmetric models with the right-handed neutrinos*, *Phys. Rev. D* **59** (1999) 116005 [[hep-ph/9810479](#)] [[INSPIRE](#)].
- [70] V. Cirigliano, B. Grinstein, G. Isidori and M.B. Wise, *Minimal flavor violation in the lepton sector*, *Nucl. Phys. B* **728** (2005) 121 [[hep-ph/0507001](#)] [[INSPIRE](#)].
- [71] G. Altarelli and F. Feruglio, *Discrete Flavor Symmetries and Models of Neutrino Mixing*, *Rev. Mod. Phys.* **82** (2010) 2701 [[arXiv:1002.0211](#)] [[INSPIRE](#)].
- [72] K.S. Babu, C.F. Kolda and J. March-Russell, *Implications of generalized $Z-Z'$ mixing*, *Phys. Rev. D* **57** (1998) 6788 [[hep-ph/9710441](#)] [[INSPIRE](#)].
- [73] B. Holdom, *Two $U(1)$'s and Epsilon Charge Shifts*, *Phys. Lett. B* **166** (1986) 196 [[INSPIRE](#)].
- [74] O. Tomalak, P. Machado, V. Pandey and R. Plestid, *Flavor-dependent radiative corrections in coherent elastic neutrino-nucleus scattering*, *JHEP* **02** (2021) 097 [[arXiv:2011.05960](#)] [[INSPIRE](#)].
- [75] S. Schlamminger et al., *Test of the equivalence principle using a rotating torsion balance*, *Phys. Rev. Lett.* **100** (2008) 041101 [[arXiv:0712.0607](#)] [[INSPIRE](#)].
- [76] E.G. Adelberger et al., *Torsion balance experiments: A low-energy frontier of particle physics*, *Prog. Part. Nucl. Phys.* **62** (2009) 102 [[INSPIRE](#)].
- [77] D.W. Hogg, *Distance measures in cosmology*, [astro-ph/9905116](#) [[INSPIRE](#)].
- [78] G. Steigman, *Primordial Nucleosynthesis in the Precision Cosmology Era*, *Ann. Rev. Nucl. Part. Sci.* **57** (2007) 463 [[arXiv:0712.1100](#)] [[INSPIRE](#)].
- [79] PLANCK collaboration, *Planck 2015 results. XIII. Cosmological parameters*, *Astron. Astrophys.* **594** (2016) A13 [[arXiv:1502.01589](#)] [[INSPIRE](#)].
- [80] S.K. Agarwalla, M. Bustamante, S. Das and A. Narang, *Present and future constraints on flavor-dependent long-range interactions of high-energy astrophysical neutrinos*, [arXiv:2305.03675](#) [[INSPIRE](#)].
- [81] PARTICLE DATA GROUP collaboration, *Review of Particle Physics*, *PTEP* **2022** (2022) 083C01 [[INSPIRE](#)].
- [82] F. Capozzi et al., *Unfinished fabric of the three neutrino paradigm*, *Phys. Rev. D* **104** (2021) 083031 [[arXiv:2107.00532](#)] [[INSPIRE](#)].
- [83] A.M. Dziewonski and D.L. Anderson, *Preliminary reference earth model*, *Phys. Earth Planet. Interiors* **25** (1981) 297 [[INSPIRE](#)].
- [84] V.D. Barger, K. Whisnant, S. Pakvasa and R.J.N. Phillips, *Matter Effects on Three-Neutrino Oscillations*, *Phys. Rev. D* **22** (1980) 2718 [[INSPIRE](#)].

- [85] H.W. Zaglauer and K.H. Schwarzer, *The Mixing Angles in Matter for Three Generations of Neutrinos and the Msw Mechanism*, *Z. Phys. C* **40** (1988) 273 [INSPIRE].
- [86] T. Ohlsson and H. Snellman, *Neutrino oscillations with three flavors in matter: Applications to neutrinos traversing the Earth*, *Phys. Lett. B* **474** (2000) 153 [hep-ph/9912295] [INSPIRE].
- [87] E.K. Akhmedov et al., *Series expansions for three flavor neutrino oscillation probabilities in matter*, *JHEP* **04** (2004) 078 [hep-ph/0402175] [INSPIRE].
- [88] S.K. Agarwalla, Y. Kao and T. Takeuchi, *Analytical approximation of the neutrino oscillation matter effects at large θ_{13}* , *JHEP* **04** (2014) 047 [arXiv:1302.6773] [INSPIRE].
- [89] S.K. Agarwalla, Y. Kao, D. Saha and T. Takeuchi, *Running of Oscillation Parameters in Matter with Flavor-Diagonal Non-Standard Interactions of the Neutrino*, *JHEP* **11** (2015) 035 [arXiv:1506.08464] [INSPIRE].
- [90] S.K. Agarwalla, S. Das, M. Masud and P. Swain, *Evolution of neutrino mass-mixing parameters in matter with non-standard interactions*, *JHEP* **11** (2021) 094 [arXiv:2103.13431] [INSPIRE].
- [91] G. Dutta, A.S. Joshipura and K.B. Vijaykumar, *Leptonic flavor violations in the presence of an extra Z*, *Phys. Rev. D* **50** (1994) 2109 [hep-ph/9405292] [INSPIRE].
- [92] I. Esteban et al., *The fate of hints: updated global analysis of three-flavor neutrino oscillations*, *JHEP* **09** (2020) 178 [arXiv:2007.14792] [INSPIRE].
- [93] *NuFIT 5.0*, (2020), <http://www.nu-fit.org/>.
- [94] Y. Farzan and S. Palomares-Ruiz, *Flavor of cosmic neutrinos preserved by ultralight dark matter*, *Phys. Rev. D* **99** (2019) 051702 [arXiv:1810.00892] [INSPIRE].
- [95] ICECUBE-GEN2 collaboration, *IceCube-Gen2: the window to the extreme Universe*, *J. Phys. G* **48** (2021) 060501 [arXiv:2008.04323] [INSPIRE].
- [96] G.J. Feldman, J. Hartnell and T. Kobayashi, *Long-baseline neutrino oscillation experiments*, *Adv. High Energy Phys.* **2013** (2013) 475749 [arXiv:1210.1778] [INSPIRE].
- [97] S.K. Agarwalla, *Physics Potential of Long-Baseline Experiments*, *Adv. High Energy Phys.* **2014** (2014) 457803 [arXiv:1401.4705] [INSPIRE].
- [98] M.V. Diwan, V. Galymov, X. Qian and A. Rubbia, *Long-Baseline Neutrino Experiments*, *Ann. Rev. Nucl. Part. Sci.* **66** (2016) 47 [arXiv:1608.06237] [INSPIRE].
- [99] C. Giganti, S. Lavignac and M. Zito, *Neutrino oscillations: The rise of the PMNS paradigm*, *Prog. Part. Nucl. Phys.* **98** (2018) 1 [arXiv:1710.00715] [INSPIRE].
- [100] O. Mena, *Unveiling neutrino mixing and leptonic CP violation*, *Mod. Phys. Lett. A* **20** (2005) 1 [hep-ph/0503097] [INSPIRE].
- [101] Y. Farzan and M. Tortola, *Neutrino oscillations and Non-Standard Interactions*, *Front. in Phys.* **6** (2018) 10 [arXiv:1710.09360] [INSPIRE].
- [102] T2K collaboration, *Measurements of neutrino oscillation parameters from the T2K experiment using 3.6×10^{21} protons on target*, arXiv:2303.03222 [INSPIRE].
- [103] NOvA collaboration, *Improved measurement of neutrino oscillation parameters by the NOvA experiment*, *Phys. Rev. D* **106** (2022) 032004 [arXiv:2108.08219] [INSPIRE].

- [104] DUNE collaboration, *Long-Baseline Neutrino Facility (LBNF) and Deep Underground Neutrino Experiment (DUNE): Conceptual Design Report, Volume 2: The Physics Program for DUNE at LBNF*, [arXiv:1512.06148](#) [INSPIRE].
- [105] DUNE collaboration, *Deep Underground Neutrino Experiment (DUNE), Far Detector Technical Design Report, Volume I Introduction to DUNE, 2020 JINST 15 T08008* [[arXiv:2002.02967](#)] [INSPIRE].
- [106] DUNE collaboration, *Deep Underground Neutrino Experiment (DUNE), Far Detector Technical Design Report, Volume II: DUNE Physics*, [arXiv:2002.03005](#) [INSPIRE].
- [107] DUNE collaboration, *Long-baseline neutrino oscillation physics potential of the DUNE experiment*, *Eur. Phys. J. C* **80** (2020) 978 [[arXiv:2006.16043](#)] [INSPIRE].
- [108] DUNE collaboration, *Low exposure long-baseline neutrino oscillation sensitivity of the DUNE experiment*, *Phys. Rev. D* **105** (2022) 072006 [[arXiv:2109.01304](#)] [INSPIRE].
- [109] M. Blennow, E. Fernandez-Martinez, T. Ota and S. Rosauero-Alcaraz, *Physics potential of the ESS ν SB*, *Eur. Phys. J. C* **80** (2020) 190 [[arXiv:1912.04309](#)] [INSPIRE].
- [110] ESSnUSB collaboration, *Updated physics performance of the ESSnUSB experiment: ESSnUSB collaboration*, *Eur. Phys. J. C* **81** (2021) 1130 [[arXiv:2107.07585](#)] [INSPIRE].
- [111] J. Conrad, A. de Gouvea, S. Shalgar and J. Spitz, *Atmospheric Tau Neutrinos in a Multi-kiloton Liquid Argon Detector*, *Phys. Rev. D* **82** (2010) 093012 [[arXiv:1008.2984](#)] [INSPIRE].
- [112] A. De Gouvêa, K.J. Kelly, G.V. Stenico and P. Pasquini, *Physics with Beam Tau-Neutrino Appearance at DUNE*, *Phys. Rev. D* **100** (2019) 016004 [[arXiv:1904.07265](#)] [INSPIRE].
- [113] A. Ghoshal, A. Giarnetti and D. Meloni, *On the role of the ν_τ appearance in DUNE in constraining standard neutrino physics and beyond*, *JHEP* **12** (2019) 126 [[arXiv:1906.06212](#)] [INSPIRE].
- [114] P. Machado, H. Schulz and J. Turner, *Tau neutrinos at DUNE: New strategies, new opportunities*, *Phys. Rev. D* **102** (2020) 053010 [[arXiv:2007.00015](#)] [INSPIRE].
- [115] S.K. Agarwalla, S. Das, A. Giarnetti and D. Meloni, *Model-independent constraints on non-unitary neutrino mixing from high-precision long-baseline experiments*, *JHEP* **07** (2022) 121 [[arXiv:2111.00329](#)] [INSPIRE].
- [116] P.F. de Salas et al., *2020 global reassessment of the neutrino oscillation picture*, *JHEP* **02** (2021) 071 [[arXiv:2006.11237](#)] [INSPIRE].
- [117] DUNE collaboration, *The DUNE Far Detector Interim Design Report Volume 1: Physics, Technology and Strategies*, [arXiv:1807.10334](#) [INSPIRE].
- [118] DUNE collaboration, *Deep Underground Neutrino Experiment (DUNE) Near Detector Conceptual Design Report*, *Instruments* **5** (2021) 31 [[arXiv:2103.13910](#)] [INSPIRE].
- [119] DUNE collaboration, *Snowmass Neutrino Frontier: DUNE Physics Summary*, [arXiv:2203.06100](#) [INSPIRE].
- [120] DUNE collaboration, *The DUNE Far Detector Interim Design Report, Volume 2: Single-Phase Module*, [arXiv:1807.10327](#) [INSPIRE].
- [121] DUNE collaboration, *The DUNE Far Detector Interim Design Report, Volume 3: Dual-Phase Module*, [arXiv:1807.10340](#) [INSPIRE].
- [122] K.T. McDonald, *An Off-axis neutrino beam*, [hep-ex/0111033](#) [INSPIRE].

- [123] T2K collaboration, *T2K neutrino flux prediction*, *Phys. Rev. D* **87** (2013) 012001 [Addendum *ibid.* **87** (2013) 019902] [[arXiv:1211.0469](#)] [INSPIRE].
- [124] P. Huber, M. Lindner and W. Winter, *Simulation of long-baseline neutrino oscillation experiments with GLOBES (General Long Baseline Experiment Simulator)*, *Comput. Phys. Commun.* **167** (2005) 195 [[hep-ph/0407333](#)] [INSPIRE].
- [125] P. Huber et al., *New features in the simulation of neutrino oscillation experiments with GLOBES 3.0: General Long Baseline Experiment Simulator*, *Comput. Phys. Commun.* **177** (2007) 432 [[hep-ph/0701187](#)] [INSPIRE].
- [126] J. Kopp, *Efficient numerical diagonalization of hermitian 3×3 matrices*, *Int. J. Mod. Phys. C* **19** (2008) 523 [[physics/0610206](#)] [INSPIRE].
- [127] J. Kopp, M. Lindner, T. Ota and J. Sato, *Non-standard neutrino interactions in reactor and superbeam experiments*, *Phys. Rev. D* **77** (2008) 013007 [[arXiv:0708.0152](#)] [INSPIRE].
- [128] S. Baker and R.D. Cousins, *Clarification of the Use of Chi Square and Likelihood Functions in Fits to Histograms*, *Nucl. Instrum. Meth.* **221** (1984) 437 [INSPIRE].
- [129] G. Cowan, K. Cranmer, E. Gross and O. Vitells, *Asymptotic formulae for likelihood-based tests of new physics*, *Eur. Phys. J. C* **71** (2011) 1554 [Erratum *ibid.* **73** (2013) 2501] [[arXiv:1007.1727](#)] [INSPIRE].
- [130] M. Blennow, P. Coloma, P. Huber and T. Schwetz, *Quantifying the sensitivity of oscillation experiments to the neutrino mass ordering*, *JHEP* **03** (2014) 028 [[arXiv:1311.1822](#)] [INSPIRE].
- [131] N. Song et al., *The Future of High-Energy Astrophysical Neutrino Flavor Measurements*, *JCAP* **04** (2021) 054 [[arXiv:2012.12893](#)] [INSPIRE].
- [132] DAYA BAY collaboration, *Precision Measurement of Reactor Antineutrino Oscillation at Kilometer-Scale Baselines by Daya Bay*, *Phys. Rev. Lett.* **130** (2023) 161802 [[arXiv:2211.14988](#)] [INSPIRE].
- [133] M. Ackermann et al., *Fundamental Physics with High-Energy Cosmic Neutrinos*, *Bull. Am. Astron. Soc.* **51** (2019) 215 [[arXiv:1903.04333](#)] [INSPIRE].
- [134] C.A. Argüelles et al., *Fundamental physics with high-energy cosmic neutrinos today and in the future*, *PoS ICRC2019* (2020) 849 [[arXiv:1907.08690](#)] [INSPIRE].
- [135] M. Ackermann et al., *High-energy and ultra-high-energy neutrinos: A Snowmass white paper*, *JHEAp* **36** (2022) 55 [[arXiv:2203.08096](#)] [INSPIRE].
- [136] P. Ballett et al., *Sensitivities and synergies of DUNE and T2HK*, *Phys. Rev. D* **96** (2017) 033003 [[arXiv:1612.07275](#)] [INSPIRE].
- [137] J. Bernabéu and A. Segarra, *Disentangling genuine from matter-induced CP violation in neutrino oscillations*, *Phys. Rev. Lett.* **121** (2018) 211802 [[arXiv:1806.07694](#)] [INSPIRE].
- [138] J. Bernabéu and A. Segarra, *Signatures of the genuine and matter-induced components of the CP violation asymmetry in neutrino oscillations*, *JHEP* **11** (2018) 063 [[arXiv:1807.11879](#)] [INSPIRE].
- [139] S.F. King, S. Molina Sedgwick, S.J. Parke and N.W. Prouse, *Effects of matter density profiles on neutrino oscillations for T2HK and T2HKK*, *Phys. Rev. D* **101** (2020) 076019 [[arXiv:2001.05505](#)] [INSPIRE].
- [140] S.K. Agarwalla et al., *Enhancing Sensitivity to Leptonic CP Violation using Complementarity among DUNE, T2HK, and T2HKK*, [arXiv:2211.10620](#) [INSPIRE].